Tracking along-arc sediment inputs to the Aleutian arc using thallium isotopes

Sune G. Nielsen [a,b,*], Gene Yogodzinski [c], Julie Prytulak [d], Terry Plank [e],
Suzanne M. Kay [f], Robert W. Kay [f], Jerzy Blusztajn [a,b], Jeremy D. Owens [a,b],
Maureen Auro [a], Tristan Kading [a]

[a] NIRVANA Laboratories, Woods Hole Oceanographic Institution, Woods Hole, MA, USA
[b] Dept. of Geology and Geophysics, Woods Hole Oceanographic Institution, Woods Hole, MA, USA
[c] Department of Earth and Ocean Sciences, University of South Carolina, Columbia, SC, USA
[d] Department of Earth Science and Engineering, Imperial College London, UK
[e] Lamont Doherty Earth Observatory, Columbia University, NY, USA
[f] Department of Earth and Atmospheric Sciences, Cornell University, Ithaca, NY, USA

Abstract

Sediment transport from the subducted slab to the mantle wedge is an important process in understanding the chemical and physical conditions of arc magma generation. The Aleutian arc offers an excellent opportunity to study sediment transport processes because the subducted sediment flux varies systematically along strike (Kelemen et al., 2003) and many lavas exhibit unambiguous signatures of sediment addition to the sub-arc mantle (Morris et al., 1990). However, the exact sediment contribution to Aleutian lavas and how these sediments are transported from the slab to the surface are still debated. Thallium (Tl) isotope ratios have great potential to distinguish sediment fluxes in subduction zones because pelagic sediments and low-temperature altered oceanic crust are highly enriched in Tl and display heavy and light Tl isotope compositions, respectively, compared with the upper mantle and continental crust.

Here, we investigate the Tl isotope composition of lavas covering almost the entire Aleutian arc a well as sediments outboard of both the eastern (DSDP Sites 178 and 183) and central (ODP Hole 886C) portions of the arc. Sediment Tl isotope compositions change systematically from lighter in the Eastern to heavier in the Central Aleutians reflecting a larger proportion of pelagic sediments when distal from the North American continent. Lavas in the Eastern and Central Aleutians mirror this systematic change to heavier Tl isotope compositions to the west, which shows that the subducted sediment composition is directly translated to the arc east of Kanaga Island. Moreover, quantitative mixing models of Tl and Pb, Sr and Nd isotopes reveal that bulk sediment transfer of ~0.6–1.0% by weight in the Eastern Aleutians and ~0.2–0.6% by weight in the Central Aleutians can account for all four isotope systems. Bulk mixing models, however, require that fractionation of trace element ratios like Ce/Pb, Cs/Tl, and Sr/Nd in the Central and Eastern Aleutians occurs after the sediment component was mixed with the mantle wedge. Models of Sr and Nd isotopes that involve sediment melting require either high degrees of sediment melting (>50%), in which case trace element ratios like Ce/Pb, Cs/Tl, and Sr/Nd of Aleutian lavas need to be produced after mixing with the mantle, or significant fluid additions from the underlying oceanic crust with Sr and Nd isotope compositions indistinguishable from the mantle wedge as well as high Sr/Nd ratios similar to that of low (<20%) degree sediment melts.

Thallium isotope data from Western Aleutian lavas exhibit compositions slightly lighter than the upper mantle, which implies a negligible sediment flux at this location and probably involvement of low-temperature altered oceanic crust in

* Corresponding author at: Dept. of Geology and Geophysics,
Woods Hole Oceanographic Institution, Woods Hole, MA, USA.
E-mail address: snielsen@whoi.edu (S.G. Nielsen).

the generation of these lavas. In general, the lightest Tl isotope compositions are observed for the highest Sr/Y ratios and most unradiogenic Sr and Pb isotope compositions, which is broadly consistent with derivation of these lavas via melting of eclogitized altered oceanic crust.

1. INTRODUCTION

Volcanic arcs are the surface expression of plate subduction, which controls the transfer of volatiles and other chemical heterogeneities into Earth's mantle. Subduction zones are also the centers of the most pronounced natural hazards on Earth due to their frequent volcanic eruptions as well as great earthquakes. It is therefore important to understand the physical and chemical mechanisms that are responsible for generating volcanic arcs.

Material erupted from arc volcanoes are derived from two principal sources: The subducting slab and the mantle wedge located between the slab and arc crust. While the mantle wedge often is considered to consist of relatively homogenous depleted peridotite, the subducting slab is highly heterogeneous, and it is uncertain which portions of it are released into the volcanic arc and which portions are ultimately subducted into the deep mantle (Ryan and Chauvel, 2014). The subducting slab contains sediments, variably altered oceanic crust (AOC), ultramafic cumulates and mantle rocks, some of which may be substantially hydrated. Uncertainties associated with determining mass fluxes from the slab make it difficult to construct models of the distribution and origin of chemical and physical heterogeneities in the deep Earth and thereby understanding mantle geodynamics and terrestrial volatile budgets.

Sediments are known to contribute to many arc lavas (Tera et al., 1986; Morris et al., 1990; Plank, 2005; Carpentier et al., 2008), but their exact fluxes from the slab are particularly difficult to quantify, in part because they likely represent a very small fraction of the material contained in arc lavas (Kay, 1980; White and Dupré, 1986; Ben Othmann et al., 1989; Thirlwall et al., 1996). Sediments may also be scraped off the slab into forearc accretionary complexes along some margins (Von Huene and Scholl, 1991). At the same time, sediments often contain very high concentrations of many trace elements compared with the mantle wedge (Ben Othmann et al., 1989; Plank and Langmuir, 1998), which could enable detection of even minor sediment additions to arc lavas. However, many of these trace elements may be strongly affected by retention in accessory mineral phases that likely exist in the slab (Johnson and Plank, 1999; Hermann and Rubatto, 2009; Skora and Blundy, 2010), which further complicates the assessment of sediment contributions to volcanic arcs.

The Aleutian arc provides an excellent opportunity to study geochemical fluxes from slab to surface because previous studies have shown that subducted marine sediments unambiguously contribute to most Aleutian lavas (Sun, 1980; Tera et al., 1986; Morris et al., 1990; Kay and Kay, 1994; Plank, 2005). In addition, there is a systematic decrease in subduction rate from east to west while only relatively minor variations occur in the overall sediment thickness subducted along the main arc (e.g. Kelemen et al., 2003). Thus, the sediment subduction flux is thought to be highest in the east and almost absent in the westernmost portions of the arc (Kay and Kay, 1994). The question, however, is whether the sedimentary flux beneath the arc is also reflected in the magnitude of the sediment component in the arc volcanic rocks and, hence, if the fraction of sediment removed from the slab to the arc is independent of total sediment subduction flux. Several studies have also suggested that the chemical characteristics of the subducted sediment are likely to change along the arc from thick continental detrital in the east (turbidites of the Zodiac and Surveyor fans) to abyssal pelagic clays in the central Aleutians (Sun, 1980; Kay and Kay, 1988, 1994; Yogodzinski et al., 2011), which should be manifested in the isotopic characteristics of Aleutian lavas. However, this trait has yet to be confirmed, partially because no direct measurements of pelagic sediments outboard of the Central Aleutians have been conducted to date.

An additional interesting feature of the Aleutian arc is the presence of lavas that may reflect melting of eclogitized subducted oceanic crust due to their high silica, high Sr/Y, and unradiogenic Pb and Sr isotope compositions (Kay, 1978; Yogodzinski et al., 1995; Yogodzinski et al., 2001; Yogodzinski et al., 2015). These lavas are predominant in the Western part of the arc with Miocene-age examples from Adak Island (Kay, 1978) giving rise to the name of the rock type adakites (Defant and Drummond, 1990).

Here we use thallium (Tl) isotope ratios to assess sediment fluxes to the Aleutian arc. Thallium isotopes have great potential to quantify fluxes from the slab because modern pelagic sediments are highly enriched in Tl and display isotopic compositions that are heavier than the isotopically homogeneous upper mantle (Rehkämper et al., 2004; Nielsen and Rehkämper, 2011; Prytulak et al., 2013). Oceanic crust altered by hydrothermal fluids at low temperatures (<100 °C), on the other hand, display light Tl isotope compositions coupled with high Tl concentrations (Nielsen et al., 2006c; Coggon et al., 2014). Therefore, the diversity of previously inferred source regions of the Aleutian arc provides an ideal setting to employ Tl isotopes as a slab component tracer.

2. THALLIUM ISOTOPE BACKGROUND

Thallium is a trace metal that displays both lithophile and chalcophile behaviors. In geochemical studies, it is often grouped with the alkali elements K, Rb, and Cs due to their similar ionic radii and charge (Shaw, 1952; Shannon, 1976; Heinrichs et al., 1980). However, a recent study found that Tl is compatible in mantle sulfides and

therefore has a higher bulk partition coefficient during mantle melting than do the alkali metals (Nielsen et al., 2014). Nonetheless, Tl is incompatible during mantle melting and is enriched in the continental crust (~300–500 ng/g) relative to the mantle (~0.5–2 ng/g) and mid ocean ridge basalts (~2–20 ng/g) (Wedepohl, 1995; Nielsen et al., 2005; Nielsen et al., 2014).

Thallium has two stable isotopes with masses 203 and 205. Thallium isotope compositions are reported relative to the NIST SRM 997 Tl standard in parts per 10,000 such that

$$\varepsilon^{205}Tl = 10,000 \times (^{205}Tl/^{203}Tl_{sample} - {}^{205}Tl/^{203}Tl_{SRM\ 997})$$
$$/(^{205}Tl/^{203}Tl_{SRM\ 997}) \qquad (1)$$

It is thought that the small relative mass difference between the two isotopes prevents extensive isotopic fractionation in all but a select few environments, which may be linked to nuclear volume isotope fractionation that occurs in chemical reactions primarily involving both oxidation states of Tl, +1 and +3 (Schauble, 2007; Nielsen and Rehkämper, 2011). Trivalent Tl, however, is not likely to be thermodynamically stable in the igneous environments including the mantle given that Tl dissolved in oxic seawater is exclusively univalent (Byrne, 2002; Nielsen et al., 2009). The univalent Tl redox state of the mantle renders the average upper mantle homogenous with respect to Tl isotopes ($\varepsilon^{205}Tl_{MORB} = -2 \pm 0.5$; (Nielsen et al., 2006b)) because no significant isotope fractionation is expected during melting or fractional crystallization (Schauble, 2007). In contrast, hydrothermally altered oceanic crust and metalliferous marine sediments are highly variable with respect to Tl isotope ratios and concentrations.

Enrichment of Tl in marine sediments is primarily due to adsorption onto authigenic manganese (Mn) oxides (Hein et al., 2000; Rehkämper et al., 2002, 2004; Nielsen et al., 2013) that precipitate ubiquitously from oxic seawater onto sedimentary particles. This adsorption process is responsible for heavy Tl isotope compositions detected in pelagic clays of $\varepsilon^{205}Tl > 2$ (Rehkämper et al., 2004) and is probably linked to surface oxidation of Tl during adsorption to Mn oxides (Peacock and Moon, 2012; Nielsen et al., 2013). Rates of Mn oxide precipitation are very slow, thus the abundance of Mn oxides in sediments generally inversely correlates with sediment depositional rates. This process renders sediments deposited close to continents or underneath highly productive water masses depleted in Tl associated with Mn oxides and consequently such sediments are characterized by $\varepsilon^{205}Tl \sim -2$, akin to the continental crust and the upper mantle (Nielsen et al., 2005, 2006b,c).

In the basaltic oceanic crust, Tl enrichment occurs within the upper few hundred meters of the oceanic crust during the circulation of seawater at low temperatures (<100 °C). Thallium enrichment may be related to biologically mediated pyrite precipitation (Coggon et al., 2014) or alternatively to Tl partitioning into alkali-rich clay minerals that also form during low temperature alteration (Nielsen et al., 2006c). Analysis of Tl concentrations and isotope compositions in low-T altered crust from IODP Hole U1301B, Deep Sea Drilling Project (DSDP) Hole 417D and DSDP/Ocean Drilling Project (ODP) Hole 504B

showed high Tl concentrations (30–1000 ng/g) and light Tl isotope ratios (down to $\varepsilon^{205}Tl \sim -15$; (Nielsen et al., 2006c; Coggon et al., 2014)). Conversely, the sheeted dike portion of the oceanic crust is depleted in Tl (<1 ng/g; (Nielsen et al., 2006c)), which is the result of hydrothermal fluid circulation at high temperature (300–400 °C) near the ridge axis that drives extraction rather than deposition of Tl. This process does not appear to cause isotope fractionation, however, as sheeted dikes have $\varepsilon^{205}Tl$ similar to MORB glass ($\varepsilon^{205}Tl \sim -2 \pm 0.5$; (Nielsen et al., 2006b; Nielsen et al., 2006c)).

The Tl isotope systematics of marine sediments and oceanic crust combined with previous studies of the Aleutian arc allow some general predictions to be made about what Tl isotope compositions to expect in different portions of the Aleutian arc. Sediment fluxes from the slab have been inferred to account for the majority of the observed trace element and isotopic enrichments in the eastern and central portions of the arc (Kay et al., 1978; Kelemen et al., 2003; Yogodzinski et al., 2011). The turbidites of the Surveyor and Zodiac fans (Fig. 1) supply primarily detrital sediments to the eastern portion of the arc, while the Central Aleutians are sufficiently distal to any continent that slowly accumulating pelagic clays become the dominant sediment type in that region. Given that Tl isotope compositions of detrital sediments ($\varepsilon^{205}Tl \sim -2$) and pelagic clays ($\varepsilon^{205}Tl > 0$) are distinct, we might expect the Central Aleutians to display somewhat heavier Tl isotope compositions than do the Eastern Aleutians. The Western Aleutians, on the other hand, are often inferred to have almost negligible sediment input. Instead, adakitic lavas that may be derived from melting of the down-going oceanic crust are common (Yogodzinski et al., 2001, 2015). If the upper volcanic portion of the oceanic crust that has previously been hydrothermally altered at low temperatures takes part in these melting processes, then Tl isotope compositions of $\varepsilon^{205}Tl < -2$ are expected.

3. SAMPLES

3.1. Aleutian lavas

Lava samples from the east and central Aleutians (from Okmok, Westdahl, Moffett and Kanaga volcanoes) were originally chosen to explore Th–Nb–REE variations with high quality ICP-MS analyses, and are the same as those published and discussed in Plank (2005) and Kay and Kay (1994). This subset of Aleutian volcanic rocks form a tight linear trend in Th/La–Sm/La that were interpreted to derive from simple binary mixing between mantle and a sedimentary component that is nearly identical to the DSDP 183 sediment average. These samples thus show clear evidence for subducting sediment in their source, largely of continental detrital (high Th/La) origin.

Western Aleutian samples were dredged from locations west of Buldir Volcano, which is the westernmost emergent volcano in the Aleutian arc (Fig. 1). The samples are from volcanic cones of the Ingenstrem Depression, a rectangular-shaped structural depression immediately west of Buldir, and from the Western Cones area, which is located 200–
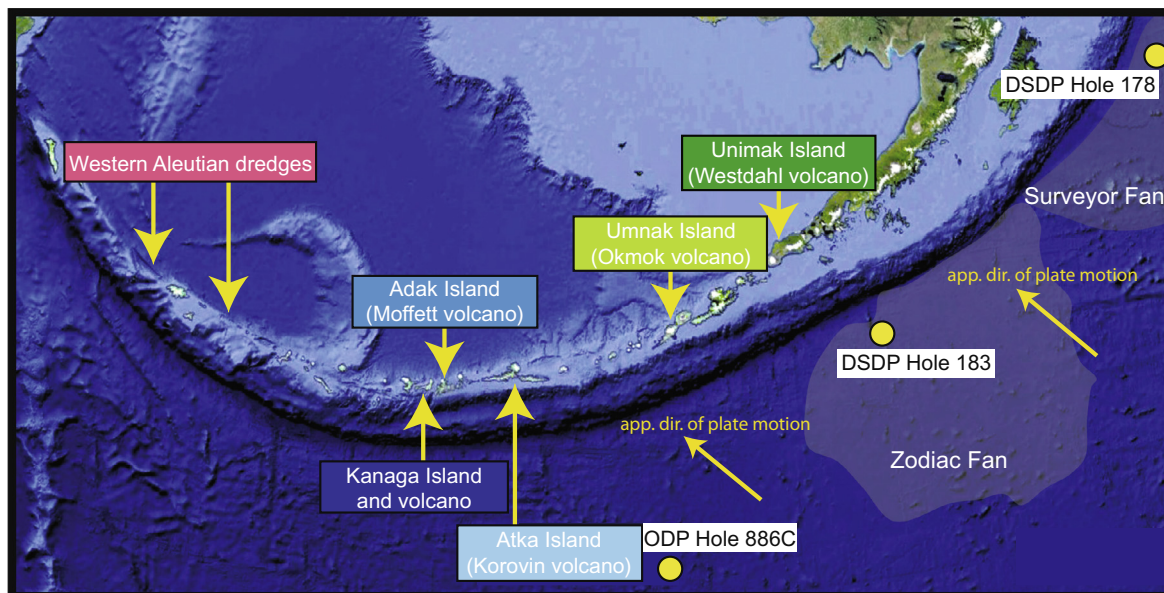
Fig. 1. Map of the Aleutian arc. Arrows indicate the locations of the lavas analyzed in this study. The colors used for the different lava locations are repeated throughout all the subsequent figures in this paper where lavas from multiple locations are plotted. Also shown are the three sediment drill cores investigated in order to characterize the sediment input flux to the arc. (For interpretation of the references to color in this figure legend, the reader is referred to the web version of this article.)

300 km further west. Ages of the samples are uncertain, but all were dredged from constructional volcanic edifices which, based on available dating, appear to be no more than 500–600 ka years old (Yogodzinski et al., 2015). Petrographic observations indicate that the samples are fresh and apparently unaffected by weathering or other alteration processes. Additional details, including geochemical methods, complete whole-rock compositions, petrographic descriptions and photomicrographs are provided in Yogodzinski et al. (2015).

3.2. Sediment samples

Thallium isotope compositions and concentrations were determined for discrete sediment samples from Deep Sea Drilling Program (DSDP) Sites 178 and 183 and Ocean Drilling Program (ODP) Hole 886C (Fig. 1).

Sites 178 and 183 are both located outboard of the eastern portion of the Aleutian arc with DSDP Site 178 located in the Gulf of Alaska and therefore slightly to the east of the Aleutian islands, but representative of sediments of the Surveyor Fan. The samples analyzed here from DSDP 178 have previously been investigated for both trace elements and some radiogenic isotope ratios (Plank and Langmuir, 1998; Vervoort et al., 2011). Samples from DSDP 183 are new samples that were obtained from core depths adjacent (2 cm) to the samples that had previously been used to assess the composition of subducted sediment in the Aleutians (Von Drach et al., 1986; Kay and Kay, 1988; Plank and Langmuir, 1998; Vervoort et al., 2011).

Sediment samples from ODP Hole 886C were also obtained, which is located outboard of the Central Aleutians on the abyssal plain at 44°41.384′N, 168°14.416′W.

The sediment thickness in this location is ∼70 m with an estimated maximum age of ∼80 Ma (Snoeckx et al., 1995). However, the upper ∼50 m were deposited in the last 10 million years while the bottom ∼20 m are characterized by several hiatuses and very slow deposition rates (Snoeckx et al., 1995). We selected 15 samples at approximately evenly distributed intervals (Table 1). Each sample was selected by visual inspection of core barrels in order to obtain the most representative samples from each section. The types of sediment analyzed range from diatom ooze to dark brown pelagic clay. Several ferromanganese (Fe–Mn) nodules are also found in Hole 886C and because such nodules often contain large enrichments of many trace metals we also selected one of these here (886C 6H-3 120–122 cm) to assess the effect on the trace element budget in the average subducted sediment composition. A single sample from the uppermost altered basaltic basement at Site 886B (Table 1) was also obtained in order to potentially assess the composition of the hydrothermally altered basaltic crust in the Central Aleutians.

4. METHODS

4.1. Sample preparation and chemical separation of Tl, Sr, Nd and Pb

The eastern and central Aleutian lavas were powdered as part of the study in Kay and Kay (1994) and Plank (2005) in an alumina ball mill to eliminate Nb–Ta contamination in samples previously powdered in tungsten carbide. Sediment samples from ODP Hole 886C were dried in an oven at 80 °C overnight before powdering in an agate swing mill. The swing mill was cleaned with high purity quartz before

Table 1
Samples selected from ODP 886C.

ODP sample ID	Depth (mbsf)	Lithology	Unit	Unit density (g/cm^3)	Unit thickness (m)
1H 3 60–62 cm	3.61	Reddish brown clay	1		
1H 4 70–72 cm	5.21	Reddish brown clay	1	1.5	6.8
2H 1 55–57 cm	7.36	Dark brown spicule clay	2		
2H 4 65–67 cm	11.96	Light brown spicule clay	2		
3H 1 90–92 cm	17.21	Brown diatom clay	2	1.45	15.4
3H 5 60–62 cm	22.91	Light brown diatom ooze	3		
4H 1 80–82 cm	26.61	Light brown diatom ooze	3		
4H 5 30–32 cm	30.61	Light brown diatom ooze	3		
5H 1 50–52 cm	35.81	Light brown diatom ooze	3		
5H 3 45–47 cm	38.76	Light brown diatom ooze	3		
6H 2 70–72 cm	47.01	Light brown diatom ooze	3	1.4	26.5
6H 3 120-122 cm	49.01	Mn nodule	4	4	0.2
7H 3 58-60 cm	57.89	Dark brown clay	5		
7H 5 73–75 cm	61.04	Dark brown clay	5	1.5	15
8H 1 48–50 cm	64.29	Dark brown clay	6		
8H 4 58-60 cm	68.89	Dark brown clay	6	1.55	8.5

and after each run, triple rinsed with deionized water and air dried to avoid cross-contamination. Lavas from the Western Aleutians consist of submarine dredges primarily from the Ingenstrom depression (~52°30′N, 175°W) were obtained as rock fragments of ~50 g. Due to potential alteration by interaction with seawater and possible contamination with Fe–Mn minerals precipitated from seawater, we did not powder these samples. Instead each sample was fractured into mm-sized chips. These were handpicked under a binocular microscope to select pieces devoid of alteration and Fe–Mn minerals. The rock chips were then ultrasonicated in MQ water to remove any dust or superficial contaminants. Additional tests were also performed on a subset of the Western Aleutian lavas in order to investigate if alteration or Fe–Mn minerals were present in the otherwise visually pure rock chips. These tests involved separating three additional aliquots of rock chips. These three splits were (1) dissolved without further preparation, (2) ultrasonicated for 1 h in 1 M distilled HCl prior to dissolution and (3) ultrasonicated for one hour in 6 M distilled HCl prior to dissolution. For two of the 1 M HCl leachates sufficient Tl was present for Tl isotope analysis.

Chips as well as powdered samples (0.1–0.3 g) were dissolved in a 1:1 mixture of concentrated distilled HF and HNO$_3$ on a hotplate overnight. Following this, they were dried and fluxed several times with concentrated distilled nitric acid and hydrochloric acid until the fluorides that formed during the first step could no longer be seen. Separate powder splits of the Central Aleutian lavas were dissolved for Tl, Sr, Nd and Pb isotopes. Following complete dissolution of fluorides, samples were dried on a hotplate and taken up in appropriate acid matrices for separation of Tl, Sr, Nd and Pb, respectively. Isolation of Tl, Sr, Nd and Pb from sample matrix followed previously published ion exchange chromatographic methods (Lugmair and Galer, 1992; Rehkämper and Halliday, 1999; Nielsen et al., 2004; Jackson and Hart, 2006; Baker et al., 2009; Scher and Delaney, 2010). Strontium was separated and purified from samples using Sr-Spec (Eichrom® Technologies, Inc.) resin. Neodymium chemistry was done

with LN resin (Eichrom® Technologies, Inc.) following methods described in Scher and Delaney (2010). Lead chemistry utilized the HBr–HNO$_3$ procedure of Lugmair and Galer (1992) and Abouchami et al., 1999. The Tl separation procedure has been shown to produce quantitative yields (Nielsen et al., 2004, 2006a; Rehkämper et al., 2004) and these can therefore be converted to Tl concentrations. Total procedural Tl blanks during this study were <3 pg, which is insignificant compared to the indigenous Tl processed for the samples of >3 ng. Total chemistry blanks for Sr, Nd and Pb were 60 pg, 5 pg and 50 pg, respectively, which is significantly less than the minimum amounts processed of 15 μg, 1 μg, and 200 ng, respectively.

4.2. Determination of Tl isotope compositions and concentrations

The Tl isotope compositions were determined at the WHOI Plasma Mass Spectrometry Facility using a Thermo Finnigan Neptune multiple collector inductively coupled plasma-mass spectrometer (MC-ICPMS). Previously described techniques that utilize both external normalization to NIST SRM 981 Pb and standard-sample bracketing were applied for mass bias correction (Rehkämper and Halliday, 1999; Nielsen et al., 2004). Due to the quantitative yields of Tl from the column chemistry procedure, Tl concentrations were determined by monitoring the ^{205}Tl signal intensities of the samples during the isotopic measurements. A known quantity of NIST SRM 981 Pb was added to the sample Tl and the measured ^{205}Tl/^{208}Pb ratios were then converted directly into Tl abundances. Previous studies (Nielsen et al., 2006b,c, 2007) that utilized the Nu Plasma MC-ICPMS applied a 5% correction that assumed Tl ionises 5% more efficiently than Pb. However, we have not been able to verify this behavior for the Neptune and thus do not apply this correction here. The uncertainty on the Tl concentration measurements is likely on the order of ±10% (2sd) (Prytulak et al., 2013). During the course of this study we evaluated the external Tl isotope reproducibility with repeat analyses of USGS reference basalt

powder BHVO-1, which was found to have an isotope composition of $\varepsilon^{205}Tl = -3.5 \pm 0.5$ (2sd) (Nielsen et al., 2015). Although individual Tl isotope analyses have internal counting statistical uncertainties of about 0.07–0.15 $\varepsilon^{205}Tl$-units (1se), we apply the external 2sd reproducibility of 0.5 $\varepsilon^{205}Tl$-units to all unknowns because this uncertainty accounts for all possible sources of error including sample dissolution, ion exchange chromatography and mass spectrometric procedures (Nielsen et al., 2004).

4.3. Determination of Sr, Nd and Pb isotope compositions

Strontium, Nd and Pb isotopic measurements were performed on a Thermo Finnigan Neptune MC-ICPMS at the WHOI Plasma Mass Spectrometry Facility. For Sr isotope measurements, isobaric interferences of ^{87}Rb on ^{87}Sr and ^{86}Kr on ^{86}Sr were corrected for by monitoring ^{82}Kr, ^{83}Kr and ^{85}Rb. Mass bias was corrected for with the exponential mass fractionation law assuming $^{86}Sr/^{88}Sr = 0.1194$, with a secondary correction to the Sr standard NIST SRM 987 ($^{87}Sr/^{86}Sr = 0.710214$) (Jackson and Hart, 2006). These secondary corrections were always smaller than 40 ppm. The internal precision for Sr isotopic measurements was 8–14 ppm (2se), while repeat measurements of the NIST SRM 987 standard yielded external precision of ∼25 ppm (2se).

For Nd isotope measurements, ^{147}Sm and ^{149}Sm were monitored to correct for the ^{144}Sm interference on ^{144}Nd. The interference corrected Nd isotope data were internally corrected for mass bias using the exponential mass bias law, assuming $^{146}Nd/^{144}Nd = 0.7219$, with a secondary correction to JNdi-1 ($^{143}Nd/^{144}Nd = 0.512104$, (Tanaka et al., 2000)). These secondary corrections were always smaller than 20 ppm. The internal precision of individual analyses was 8–12 ppm (2se) and the external precision, assessed through repeat analyses of JNdi-1, was ∼ 15 ppm (2se).

Lead isotope compositions were externally normalized for instrumental mass bias relative to $^{205}Tl/^{203}Tl = 2.3871$ for the NIST SRM 997 Tl standard and were also corrected using measurements of NIST SRM 981 using values from Todt et al. (1996). The Pb isotopic ratios have internal precision of 15–60 ppm for $^{206}Pb/^{204}Pb$, $^{207}Pb/^{204}Pb$, and $^{208}Pb/^{204}Pb$. External reproducibility was assessed through repeat measurements of NIST SRM 981 and range from 17 ppm (2se) for $^{207}Pb/^{206}Pb$ to 120 ppm (2se) for $^{208}Pb/^{204}Pb$.

The well-characterized USGS rock standard BHVO-1 was dissolved, processed, and analyzed along with unknowns. Results for Pb, Sr and Nd isotopic measurements of the BHVO-1 rock standard (Table S1) are within error of those reported in Weis et al. (2005, 2006).

4.4. Trace element concentration analyses

The Eastern and Central Aleutian lavas were digested and analyzed by ICP-MS, as described and given in Plank (2005). DSDP 183 and 178 sediments were analyzed by INAA, DCP and ICP-MS sediments as described and presented in Kay and Kay (1988), Plank and Langmuir (1998) and Vervoort et al. (2011), respectively. The ODP 886C sediments were analyzed by ICP-MS and ICP-ES at Lamont-Doherty Earth Observatory as part of this study, following procedures described in Rabinowitz et al. (2015). Calibration standards and data quality are as reported in Rabinowitz et al. (2015). Notably, thallium concentrations were determined to within 3% relative standard deviation based on three separate digestions of the Indian Ocean Radiolarian Clay (407 ± 11 ng/g).

5. RESULTS

Thallium isotopic variation in the Eastern and Central Aleutian Islands (Unimak to Kanaga, Fig. 1) ranges from $\varepsilon^{205}Tl = -3.8$ to $+2.6$ (Table 2). The vast majority of samples, however, have values that are within error of or heavier than the average upper mantle and continental crust ($\varepsilon^{205}Tl = -2$). The largest spread in Tl isotope compositions are found in samples from Adak and Kanaga islands whereas samples in the eastern Aleutians tend to cluster around the value for average upper mantle and continental crust ($\varepsilon^{205}Tl = -2$). Samples in this study from Adak and Kanaga islands also cover the largest range in age (Kay and Kay, 1994), which may partially account for the larger Tl isotope diversity. For the most mafic lavas ($SiO_2 < 54\%$), Tl concentrations range between 25 and 97 ng/g, which is significantly enriched compared to 2–20 ng/g observed for most MORB (Jenner and O'Neill, 2012; Nielsen et al., 2014).

Lavas from the Western Aleutians are characterized by lighter Tl isotope compositions than the Central and Eastern Aleutians with most samples exhibiting $\varepsilon^{205}Tl = -3.4$ to -1.5. Two samples have somewhat heavier Tl isotope compositions close to $\varepsilon^{205}Tl = 0$ while one sample is very light at $\varepsilon^{205}Tl = -9.3$ (Table 3). Thallium concentrations in the Western Aleutian lavas overlap with those recorded for basaltic samples from the Eastern and Central Aleutians, but also extends up to 470 ng/g for the very light sample. It is important to note that repeat analyses of Western Aleutian lavas often showed a range of concentrations (Table 3). Some of this variation can possibly be ascribed to the presence of contamination from Fe–Mn minerals or alteration via interaction with seawater. However, a large fraction of this variation is clearly unrelated to these secondary processes as the four different analyses of sample TN182_07_002 varies by more than a factor of five (Table 3). The most likely explanation for the large concentration differences is that the Western Aleutian rocks are crystalline with a mixture of mineral grains up to several mm in diameter and groundmass (Yogodzinski et al., 2015). Each Tl isotope analysis was performed on separately handpicked rock chips, not from a homogenized rock powder. Most igneous minerals (olivine, pyroxene, plagioclase, amphibole) likely contain very low Tl concentrations (Adam and Green, 2006) and, hence, it is expected that samples are heterogeneous on the mm-scale with respect to Tl concentrations. With this caveat in mind, we emphasize that element ratios involving Tl for Western Aleutian samples likely have uncertainties that approach a factor of two. All other Tl isotope analyses were performed on homogenous rock powders and are therefore not prone to effects of heterogeneity.

Table 2
Tl, Sr, Nd and Pb isotopes for main arc lavas.

Sample	ε^{205}Tl	Tl [ng/g]	n	^{87}Sr/^{86}Sr	^{143}Nd/^{144}Nd	^{206}Pb/^{204}Pb	^{207}Pb/^{204}Pb	^{208}Pb/^{204}Pb
Kanaga 514	0.2	20	1	0.70307	0.51303	18.731	15.545	38.259
repeat	0.5	31	2					
Kanaga 58	−1.6	199	1	0.70330	0.51304	18.802	15.558	38.347
Kanaga S489	−3.4	24	1	0.70307	0.51301	18.734	15.548	38.267
repeat	−4.1	25	2					
Kanaga S508	0.8	40	1	0.70308	0.51302	18.731	15.548	38.268
Moffett 18–15A	1.2	26	1	0.70312	0.51300	18.710	15.538	38.220
Moffett 18–15B	1.3	32	1	0.70312	0.51301	18.709	15.539	38.222
Moffett 2A	2.6	43	1	0.70314	0.51299	18.705	15.540	38.220
Moffett 81 19A	1.8	37	1	0.70315	0.51302	18.731	15.545	38.260
Moffett ADK53[*]	−3.3	34	1	*0.70285*	*0.51309*	*18.462*	*15.499*	*37.964*
Okmok UM-10	0.7	36	1	0.70303	0.51304	18.726	15.545	38.245
Okmok UM-21	−1.7	91	1	0.70325	0.51304	18.877	15.569	38.415
Okmok UM-23	−0.5	97	1	0.70326	0.51303	18.865	15.566	38.404
Okmok UM-5	−0.2	59	1	0.70329	0.51302	18.887	15.570	38.430
repeat	−0.2	60	2					
Westdahl SAR-4	−2.1	170	1	0.70304	0.51307	18.859	15.561	38.388
Westdahl SAR-11	−1.4	68	1	0.70313	0.51304	18.867	15.563	38.403
Westdahl SAR-17	−1.4	27	1	0.70309	0.51304	18.870	15.562	38.398
repeat	−1.6	32	2					
Westdahl SAR-7	0.1	56	1	0.70313	0.51306	18.872	15.563	38.398
KR01-20	−2.0	43	1		0.51302	18.839	15.573	38.408
KRO1-6_11	0.5	41	1	0.70323	0.51304	18.791	15.557	38.341
repeat	0.7	45	2					
KR01-37_23	0.0	81	1	0.70349	0.51302	18.843	15.577	38.418
repeat	0.5	80	2					
KRO2-55_8	−2.0	115	1		0.51303	18.825	15.571	38.389
KR01-33_14	−2.3	165	1		0.51302	18.826	15.570	38.391
KR02-74_17	−0.9	194	1		0.51301	18.846	15.576	38.419
KR01-9_26	−2.3	244	1		0.51303	18.849	15.576	38.421
KR01-24_29	−2.1	297	1		0.51302	18.846	15.574	38.414

[*] Radiogenic isotope data from (Kay, 1978; Sun, 1973).

Sediments outboard of the Aleutian arc display Tl isotope compositions from ε^{205}Tl = −3.1 to +10.9 (Table 4), while Tl concentrations also vary strongly between 55 and ~20,000 ng/g. Although most samples fall in the range from ε^{205}Tl = −3 to −1, there is a clear tendency for the most Tl-rich samples to display the heaviest Tl isotope compositions (Fig. 2). In addition, it is evident that samples from ODP Site 886C exhibit, on average, heavier Tl isotope compositions and higher Tl concentrations than do the sediments from DSDP 178 and 183 (Fig. 2), which is clearly related to the high abundance of Fe–Mn minerals in certain sections of ODP Site 886C sediments. Another striking feature of the pelagic sediments from ODP Site 886C outboard of the Central Aleutians is that ^{206}Pb/^{204}Pb and ^{208}Pb/^{204}Pb isotope compositions of many samples are significantly less radiogenic than those found in DSDP Holes 178 and 183 that are further to the east (Table 4). This effect is likely due to the presence of Pb-rich Fe–Mn minerals that precipitate directly from North Pacific seawater, which is thought to have been unradiogenic throughout the Cenozoic (Ling et al., 1997; Ling et al., 2005). In addition, the oldest and most Pb-enriched pelagic sediments in Hole 886C also display very unradiogenic ^{207}Pb/^{204}Pb, which could indicate Pb inputs to seawater from MORB hydrothermal sources

at this location. However, due to the large uncertainties on the sediment ages in the lower portion of ODP Hole 886C (Snoeckx et al., 1995) it is difficult to assess to what extent these sediments contain sufficient Pb to significantly affect the bulk subducted sediment ^{207}Pb/^{204}Pb isotope composition.

Here we use the trace element concentrations and isotope compositions determined for sediments outboard of the Aleutian Islands to construct weighted average subducted sediment compositions for the eastern and central Aleutians (Table 5). The averages were also weighted by lithological abundance and density (Table 1), which was determined based on sediment descriptions and core barrel photographs (Rea et al., 1993). It is assumed that the sediment pile found at ODP Hole 886C is similar to what has been subducted in the Central Aleutians for the past at least 10 Ma. This assumption is reasonable because the sediment depositional environments as a function of distance from the Aleutian arc in the direction of the plate motion have likely remained relatively constant over this time period. That is, the North Pacific is characterized by relatively high productivity resulting in diatom rich sediments whereas the Central Pacific gyres display low productivity and, therefore, are dominated by abyssal red clays. Below we use

Table 3
Tl concentrations and isotopic compositions of Western Aleutian lavas.

Sample	tn182_01_001	tn182_01_007	tn182_03_002	tn182_04_003	tn182_05_001	tn182_07_002	tn182_07_005	tn182_07_009	tn182_08_003	tn182_08_013	tn182_08_014	tn182_09_001	tn182_10_003	tn182_10_004	tn182_11_001	tn182_11_004	tn182_13_001	SO201-1b-33–001	SO201-1b-35–004	SO201-1b-36–003
ultrasonic H2O																				
ε^{205}Tl	−3.2	−2.2	−2.2	−2.7	−2.6	−0.5	0.6	−2.7	−9.3	−2.3	−1.7	−1.5	−0.7	−3.4	−2.2	−2.0	−1.8	−3.1	−2.3	−1.3
Tl [ng/g]	110	59	54	65	54	69	23	151	476	69	66	83	124	298	123	79	94	56	48	33
Ultrasonic 1M HCl																				
ε^{205}Tl						−1.8	0.9		−9.2				0.6							
Tl [ng/g]						107	30		465				113							
Ultrasonic 6M HCl																				
ε^{205}Tl						−1.8	0.7	−2.5					−1.0							
Tl [ng/g]						106	30	184					160							
No treatment																				
ε^{205}Tl						0.3	2.2		−9.5				−0.6							
Tl [ng/g]						17	23		877				162							
1M HCl leach																				
ε^{205}Tl						9.8			0.3											
Tl [ng/g]						2			9											
Preferred Values																				
ε^{205}Tl	−3.2	−2.2	−2.2	−2.7	−2.6	−1.8	0.7	−2.6	−9.3	−2.3	−1.7	−1.5	−0.4	−3.4	−2.2	−2.0	−1.8	−3.1	−2.3	−1.3
Tl [ng/g]	110	59	54	65	54	107	27	168	470	69	66	83	140	298	123	79	94	56	48	33

Table 4
Geochemical data for sediments outboard of the Aleutian arc.

Site	Core	Section	Interval (cm)	Description	ε206Tl	87Sr/86Sr	143Nd/144Nd	206Pb/204Pb	207Pb/204Pb	208Pb/204Pb	Li	Be	Sc	V	Cr	Co	Ni	Cu	Ga	Zn	Rb	Sr	Y	Zr	Nb	Cs	Ba	La	Ce	Pr	Nd	Sm	Eu	Tb	Gd	Dy	Ho	Er	Yb	Lu	Hf	Ta	Tl	Pb	Th	U	ICP-ES	TiO2	Al2O3	MnO	Fe2O3	MgO	CaO	Na2O	K2O	P2O5
178	1	1	88–94	Silty clay	−2.6																																						0.42													
178	12	2	112–117	Silty clay	−2.4																																						0.32													
178	24	3	87–92	Silty clay/pebbles	−2.3																																						0.055													
178	29	5	129–134	Silty clay	−1.6																																						0.058													
repeat 178	39	5	108–110	Volcanic ash	−1.4																																						0.060													
178	39			Volcanic ash	−1.5																																						0.261													
178	47	1	127–130	Silt/v. fine sand	−2.2																																						0.41													
178	47	1	141–145	Silt/v. fine sand	−2.5																																						0.62													
178	57	1	136–140	Clay shale	−0.8																																						0.039													
183	2R	3	52–54	Diatom rich silty clay	−1.8																																						0.28													
183	9R	3	82–84	Clayey diatom ooze	−2.1																																						0.27													
183	17R	3	72–74	Diatom ooze	−1.2																																						0.066													
183	21R	1	129–131	Clay bearing diatom ooze	1.0																																						0.173													
183	22R	2	95–97	Silty clay	2.0																																						0.55													
183	24R	3	85–87	Clay	−3.1																																						0.42													
183	27H	3	36–38	Silt	−2.6																																						0.34													
183	27H	3	101–103	Clay	−2.6																																						0.39													
183	31R	1	52–54	Silty sand	−2.5																																						0.30													
183	38R	2	68–70	Clay	−2.9																																						0.40													
183	39R	1	17–19	Silty clay	−2.9																																						0.36													
183	39R	1	97–99	Limestone	−0.4																																						1.78													
886C	1H	3	60–62	Reddish brown clay	0.6	0.70074	0.51238	18.740	15.636	38.811	40.6	2.62	25.2	116	50.0	49.6	59	187	59	115	95	198	21.5	121	9.85	8.55	2912	26.1	69.96	7.9	29.28	6.99	1.75	6.12	0.99	5.19	0.96	2.56	2.39	0.37	3.06	0.74	0.71	27.6	11.90	1.80		0.68	12.71	0.43	6.11	2.72	1.65	4.30	2.52	0.10
886C	1H	4	70–72	Reddish brown clay	0.9	0.71178	0.51231	18.727	15.640	38.830	41.7	2.36	19.6	95	48.3	42.5	68	166	57	106	93	160	16.2	105	9.42	9.01	2801	22.1	60.17	5.9	21.35	4.72	1.16	4.07	0.66	3.50	0.68	1.87	1.84	0.29	2.66	0.69	0.67	24.6	9.76	1.64		0.53	11.10	0.39	4.99	2.37	0.95	4.07	2.31	0.07
886C	2H	1	55–57	Dark brown spicule clay	−0.2																																																			
886C	2H	4	65–67	Light brown spicule clay	−1.7																																																			
886C	3H	5	90–92	Brown diatom clay	−1.2	0.71240	0.51229	18.726	15.643	38.853	42.7	3.00	24.0	91	51.2	60.0	108	225	110	123	109	197	17.4	142	11.65	10.27	5908	24.5	73.84	6.7	24.15	5.64	1.53	4.78	0.78	4.12	0.79	2.18	2.21	0.35	3.33	0.87	0.65	28.5	13.14	2.06		0.57	11.62	0.52	5.12	2.43	0.78	3.81	2.59	0.04
886C	3H		60–62	Light brown diatom ooze	−2.0						13.1	0.94	9.1	25	18.9	5.6	35	120	51	58	34	79	5.1	41	3.32	3.29	2995	8.2	24.18	2.3	7.78	1.86	0.49	1.52	0.24	1.25	0.23	0.63	0.65	0.10	0.90	0.23	0.170	7.0	4.07	0.59		0.16	3.43	0.03	1.54	1.09	0.30	3.47	0.84	0.01
886C	4H	1	80–82	Light brown diatom ooze	−2.0																																																			
886C	4H	5	30–32	Light brown diatom ooze	−1.7						21.7	1.60	14.3	53	15.1	212	175	232	44	266	41	127	11.7	106	3.87	3.33	2302	8.6	24.44	2.6	9.68	2.52	0.69	2.41	0.40	2.30	0.47	1.31	1.34	0.21	2.34	0.26	0.206	28.8	3.84	0.96		0.42	6.78	0.06	6.11	2.19	1.49	4.21	1.38	0.08
886C	5H	1	50–52	Light brown diatom ooze	−0.5																																																			
886C	5H	3	45–47	Light brown diatom ooze	−1.3																																																			
886C	6H	2	70–72	Light brown diatom ooze	−1.1																																																			
886C	6H	3	120–122	Mn nodule	10.9	0.70924	0.51246	18.606	15.630	38.739	12.4	5.28	13.3	62	10.2	2969	2234	3422	40	327	26	665	64.5	613	20.29	2.57	2497	154.5	1341.03	58.7	221.21	59.17	14.23	48.44	8.46	39.36	6.44	15.46	13.98	2.02	11.51	0.17	4.04	22.6	84.96	5.72		1.04	4.46	10.51	14.50	1.85	1.36	2.40	0.94	0.12
repeat 886C					10.6																																																		
886C	7H	3	58–60	Dark brown clay	3.3			18.621	15.628	38.762	63.6	3.35	42.9	107	53.2	180.9	311	578	119	174	121	254	82.5	254	15.81	11.49	6216	55.7	195.51	20.5	82.35	22.43	5.77	21.11	3.46	18.61	3.54	9.45	9.14	1.47	6.32	1.06	1.62	48.9	21.16	3.15		0.72	15.57	1.66	6.65	3.08	1.18	3.31	3.49	0.29
repeat					3.7			18.58	15.621	38.697																																												
886C	7H	5	73–75	Dark brown clay	2.5			18.569	15.598	38.564																																													
886C	8H	1	48–50	Dark brown clay	3.7	0.71003	0.51239	18.569	15.599	38.907	36.4	3.34	38.8	393	43.1	121.3	420	597	21	355	74	302	329.0	265	17.31	5.93	593	212.2	248.10	67.6	278.62	66.25	16.29	67.95	10.69	59.87	11.98	31.78	27.04	4.19	7.03	0.86	5.27	84.3	13.95	4.25		0.84	12.01	2.73	15.53	3.02	3.44	2.74	2.91	2.34
repeat 886C								18.70	15.599	38.907																																												
886C	8H	4	58–60	Dark brown clay	6.4			18.416	15.522	38.002	21.8	6.34	22.5	846	14.5	72.7	685	1211	25	850	28	492	373.3	271	9.68	2.22	1394	359.5	93.01	113.7	462.77	106.55	25.68	103.40	15.99	85.62	16.34	41.45	33.56	4.89	4.82	0.36	20.67	146.3	4.07	6.24		0.34	5.91	8.24	35.45	2.39	2.20	2.24	1.34	1.77
886B	9X	1	60–62	Highly altered basalt, brown	−2.7			19.082	15.627	38.367	23.9	0.99	30.2	171	613	50.7	180	149	12	191	26	177	19.9	83	1.02	0.70	48	8.9	8.02	2.9	12.49	3.63	1.38	4.59	0.80	4.80	0.94	2.44	2.06	0.30	2.25	0.09	1.12	2.01	0.068	0.90		1.31	21.17	0.17	11.55	1.71	6.57	2.95	0.20

Trace element and radiogenic isotope data from DSDP 178 and DSDP 183 from Plank and Langmuir (1998) and Kay and Kay (1988).
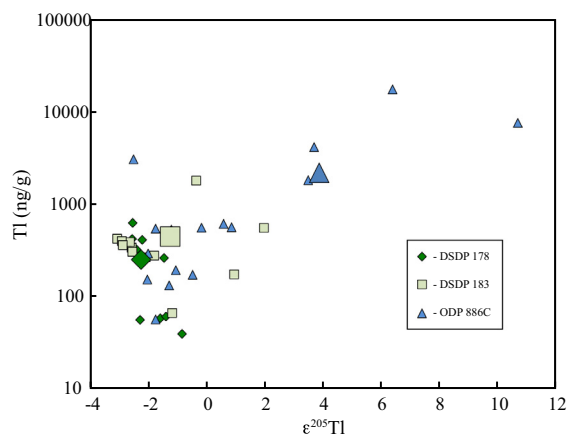
Fig. 2. Thallium isotope composition and concentration for individual sediment samples from DSDP 178 (dark green), DSDP 183 (light green) and ODP 886C (blue). These colors mimic those used for the lavas whereby the eastern-most sediment core is dark green followed by light green and blue. The large symbols indicate the concentration weighted average Tl isotope compositions and concentrations for each of the three sediment cores. Although DSDP 183 and ODP 886C both contain pelagic components with heavy Tl isotopes and detrital components with ε^{205}Tl ~ -2, ODP 886C clearly is much more dominated by the pelagic components than DSDP 183. (For interpretation of the references to color in this figure legend, the reader is referred to the web version of this article.)

Table 5
Weighted average subducted sediment components.

Parameter[*]	East Aleutian Sediment[#]	Cent. Aleutian Sediment
Rb	57	77.1
Cs	3.4	7.1
Sr	245	203
Ba	2074	3910
La	18.0	58.8
Ce	39.0	103
Nd	19.1	75.7
Tl	0.31	2.25
Pb	12.9	39.6
Th	5.5	11.4
U	2.4	2.23
^{87}Sr/^{88}Sr	0.7064	0.711
^{143}Nd/^{144}Nd	0.51261	0.5124
^{206}Pb/^{204}Pb	19.04	18.61
^{207}Pb/^{204}Pb	15.63	15.61
^{208}Pb/^{204}Pb	38.69	38.60
ε^{205}Tl	−2.0	3.9

[*] Concentrations in µg/g.
[#] Eastern Aleutian sediment composition from Plank and Langmuir, 1998 except Nd isotope composition from Vervoort et al. (2011) and Tl concentrations and isotopes (This study).

the average subducted sediment components to investigate how changing sediment composition along the Aleutian arc affects the composition of erupted lavas.

6. DISCUSSION

6.1. Thallium isotopic variation induced by secondary processes

The Tl isotope compositions and concentrations recorded in volcanic rocks can be modified by a number of syn- and post-eruption processes such as degassing, sub-aerial aqueous alteration, submarine hydrothermal alteration and submarine precipitation of Fe–Mn minerals on sample surfaces. In addition, assimilation of wall rock and fractional crystallization prior to eruption could also alter the Tl budget of the original magma if the Tl concentrations and/or isotope compositions of wall rock and crystallizing phases were different from that of the original magma. In the following sections we discuss the potential for these processes to have affected our Tl isotopic data for lavas from the Aleutian arc in order to assess how much Tl isotope variation can be directly linked to inputs from the subducted slab.

6.1.1. Submarine contamination and alteration of Western Aleutian samples

Lavas erupted under submarine conditions are easily contaminated with Tl either associated with clay minerals that form during alteration of the lava (Jochum and Verma, 1996) or due to precipitation of Fe–Mn oxyhydroxides that form ubiquitously in oxic seawater (Nielsen and Rehkämper, 2011). As outlined in Section 2, both these components are characterized by very strong Tl enrichments compared with those found in mantle derived melts as well as substantial Tl isotope fractionation (Rehkämper et al., 2004; Nielsen et al., 2006c; Coggon et al., 2014). Thus, even minute amounts of these contaminants may completely alter the Tl concentration and isotope composition of a given sample. In order to eliminate these sources of contamination, we analyzed only rock chips of dredge samples (not powders), which were prepared as described above to eliminate possible effects of seawater–rock interaction. The results of these analyses reveal Tl isotope and concentration patterns for a few samples that could reflect alteration or Fe–Mn mineral contamination. Additional tests were, therefore, conducted on a subset of the samples to further investigate if contamination was significant (Table 3). These tests involved leaching two separate aliquots of chips in 1 M HCl and 6 M HCl, respectively, during ultrasonication. The results of these tests confirm that one sample (TN182_07_002) had clearly been affected by minor Fe–Mn mineral contamination. This assessment was confirmed by analysis of both an untreated aliquot of the sample as well as the 1 M HCl leachate, both of which showed heavy Tl isotope compositions as would be expected for Fe–Mn minerals (Rehkämper et al., 2002; Peacock and Moon, 2012; Nielsen et al., 2013). It is notable that even though the 1 M HCl leachate contained only very small amounts of Tl (2 ng per gram of sample) the exceedingly heavy Tl isotope composition of the leachate (ε^{205}Tl = +9.8), which is consistent with values found in Fe–Mn crusts (Rehkämper et al., 2002; Nielsen et al., 2009, 2011), approximately accounts for the small isotopic

shift observed in the unleached samples. The uncontaminated Tl isotope composition of the sample is, therefore, best represented by the leached aliquots both of which display identical values of $\varepsilon^{205}Tl = -1.8$. We are confident that the leaching process has not induced notable Tl loss or isotope fractionation in sample TN182_07_002 because leaching of an uncontaminated sample (TN182_07_009) yielded a result identical to the untreated sample aliquot (Table 3).

6.1.2. Degassing

Degassing should be expressed as a loss of Tl potentially associated with kinetic isotope fractionation whereby the light Tl isotope would preferentially be lost. Thallium isotope measurements of volcanic fumaroles did not find any systematic enrichment in ^{203}Tl (Baker et al., 2009), suggesting that kinetic Tl isotope fractionation during degassing might be limited. However, these effects have never been investigated for actual rocks, which makes it difficult to predict the magnitude of Tl isotope and concentration effects from degassing.

Given that Tl partitioning during mantle melting is similar to that of Ce (Nielsen et al., 2014), it could be inferred that unusually high Ce/Tl ratios coupled with heavy Tl isotope compositions might be indicative of significant degassing. However, because Ce/Tl in both sediments and AOC (Ce/Tl ∼ 100–400) is much lower than the upper mantle (Ce/Tl ∼ 1100, (Nielsen et al., 2014)) variations in Ce/Tl are not necessarily due to degassing unless Ce/Tl significantly exceeds the mantle value. Except for three samples, all Aleutian lavas display Ce/Tl ratios significantly lower than the upper mantle (Fig. 3). In addition all samples fall within the field expected for mixing between the mantle and sediments or AOC (Fig. 3), which suggests that degassing did not significantly affect Tl concentrations or isotopes in the majority of the samples studied here.

Of the three samples that display significantly higher Ce/Tl than sediments and AOC, one (SAR-17) displays Ce/Tl and ε^{205}Tl within error of the upper mantle, which could be consistent with a melt largely unmodified by addition of slab material. However, Pb isotope ratios in SAR-17 and other samples from this volcano are much more radiogenic (Table 2) than the depleted MORB mantle (Workman and Hart, 2005), which likely reflects the influence of terrigenous sediments (Kay et al., 1978). Alternatively, the low Tl content of this sample may reflect degassing from a lava that either (1) had a starting Tl isotope composition significantly lighter than the normal mantle or (2) did not register any significant Tl isotope fractionation during degassing. The latter interpretation would be consistent with the data of Baker et al. (2009), which showed no systematic enrichment in ^{203}Tl for volcanic fumaroles.

The second sample (TN182_07_005) with Ce/Tl similar to the upper mantle is characterized by ε^{205}Tl significantly heavier than the upper mantle (Table 3), which is consistent with degassing coupled with kinetic Tl isotope fractionation. This conclusion is supported by the chemical compositions of samples TN182_07_009 and TN182_07_005, which were collected in close proximity to one another, being almost identical for all elements except Tl concentra-
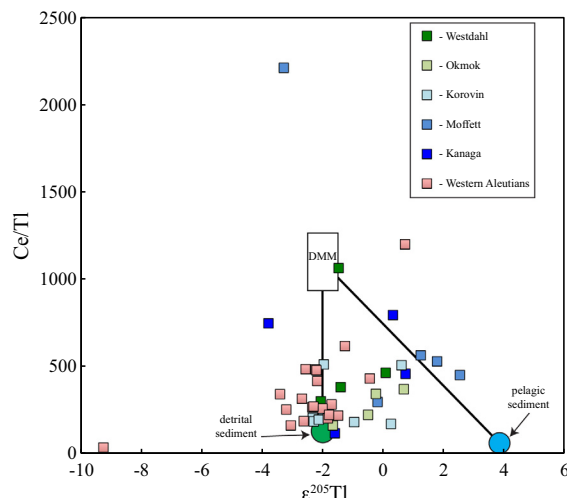
Fig. 3. Ce/Tl ratios plotted against Tl isotope composition for all Aleutian lavas investigated in this study. Also shown is the depleted mid ocean ridge basalt mantle (DMM) as well as the average compositions for detrital (DSDP 178 and 183) and pelagic (ODP 886C) sediments. Note that the legend colors follow that of the map in Fig. 1 and is the same for all subsequent figures with lavas from multiple locations. (For interpretation of the references to color in this figure legend, the reader is referred to the web version of this article.)

tions and isotopes. It is unclear exactly why Tl isotopes are significantly different for these two samples, but, given the anomalous Tl isotope composition, we infer that TN182_07_005 was likely degassed and does not reflect the primary Tl isotope systematics of the original lava. Therefore, we will not consider it further in our discussion of slab-mantle interactions in the Aleutian arc and it has not been included in any figure except Fig. 2.

The last sample to display Ce/Tl higher than the upper mantle is the Miocene adakite lava from Mt. Moffett (ADK53), which could indicate significant Tl degassing. However, the Tl isotope composition of ADK53 is not enriched in ^{205}Tl (Table 2), as might be expected from kinetic isotope fractionation. In addition, this sample has, based on its high Sr/Y and unradiogenic Sr and Pb isotope ratios, been proposed as a possible melt derived from eclogitized oceanic crust (Kay, 1978). Bulk Tl and Ce partition coefficients during melting of eclogite are unlikely to be identical to those found for mantle melting and therefore it is possible that Ce/Tl could be significantly altered during eclogite melting. Thallium partitions into sulfide (Kiseeva and Wood, 2013; Nielsen et al., 2014) and probably phengite (Prytulak et al., 2013) while Ce may be accommodated by allanite and/or epidote (Hermann, 2002; Carter et al., 2015). The relative abundances of these minerals will have a strong control on melt Ce/Tl especially at low degrees of melting where these phases potentially could be in the residue. However, given the lack of experimental data on Tl partitioning at relevant conditions it is currently not possible to constrain the effect on Ce/Tl during eclogite melting. Therefore, it we cannot conclusively distinguish between degassing or source mineralogy as the cause of the high Ce/Tl observed in ADK53.

For the remaining samples in this study we do not find any chemical or isotopic indications of significant degassing. If Tl degassing played a role in the Tl budgets of the lavas investigated here, then the effects are too small to quantify and most likely smaller than the Tl elemental and isotopic signatures imposed by addition of subduction components.

6.1.3. Subaerial aqueous alteration

Subaerial lavas are often observed to preferentially lose alkali metals during aqueous alteration from meteoric water (Schiano et al., 1993). This effect is most likely due to the high solubility of these metals in aqueous solution and given the geochemical similarity between Tl and the alkali metals (i.e. ionic charge and radius as well as high aqueous solubility) one might expect subaerial alteration to be accompanied by significant Tl losses that would lead to high Ce/Tl ratios. These losses, however, would likely not be associated with Tl isotope fractionation because weathering has been shown to cause negligible Tl isotope fractionation (Nielsen et al., 2005).

High Ce/Tl ratios produced by subaerial weathering should be coupled with significant losses of alkali metals. Here we investigate this using Th/Rb as these two elements partition similarly in igneous processes while Th is highly insoluble in aqueous solution. Thus, high Th/Rb coupled with high Ce/Tl might indicate subaerial alteration. Fig. 4 shows that only sample ADK53 has a clear signature that could be interpreted as subaerial alteration. Some alteration of ADK53 is also reasonable given that it is Miocene in age. All other samples investigated here are relatively recent, fresh lava flows that are unlikely to have experienced significant alteration. It should be noted that, while the trace element systematics of mobile elements like K, Rb, Cs and Tl may have been perturbed in ADK53, there is no indication that the original isotope compositions (radiogenic or Tl) of this lava have been reset by post-eruption processes. We, therefore, use the isotopic characteristics of ADK53 in our discussion of subduction processes in the Aleutian arc, but omit trace element ratios from consideration.

6.1.4. Assimilation and fractional crystallization

Fractional crystallization in itself is not likely to alter the Tl isotope composition of magma. First, Tl is likely very incompatible in the major crystallizing phases like olivine, clinopyroxene and plagioclase (Adam and Green, 2006; Nielsen et al., 2014). Second, lavas from Korovin volcano (Atka Island) also support the lack of Tl isotope fractionation with magmatic differentiation. These Korovin lavas display patterns broadly consistent with evolution by fractional crystallization from basalt to high-silica andesite (Fig 5). Thallium is enriched in the more evolved lavas and the progressive Tl enrichment is not accompanied by any systematic Tl isotope change (Table 2), which confirms that fractional crystallization does not impart any detectable Tl isotope fractionation. The constancy of Tl isotopes for the more evolved samples also shows that any assimilation that might have occurred during fractional crystallization of the Korovin samples did not cause a notable change in Tl isotopes.
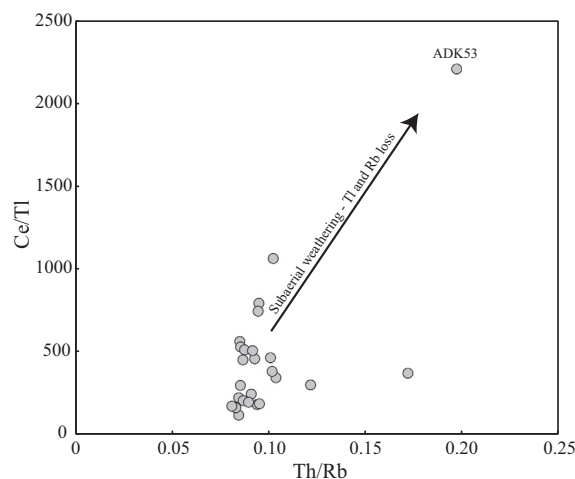
Fig. 4. Ce/Tl plotted against Th/Rb for all subaerial lavas analyzed in this study. Subaerial aqueous alteration of basaltic lavas preferentially removes alkali metals and given the similarity of the ionic charge and radius between Tl and the alkali metals similar loss of Tl is likely during subaerial alteration. Hence, samples with high Ce/Tl and Th/Rb are probably affected by post eruption alteration (see text for further details).
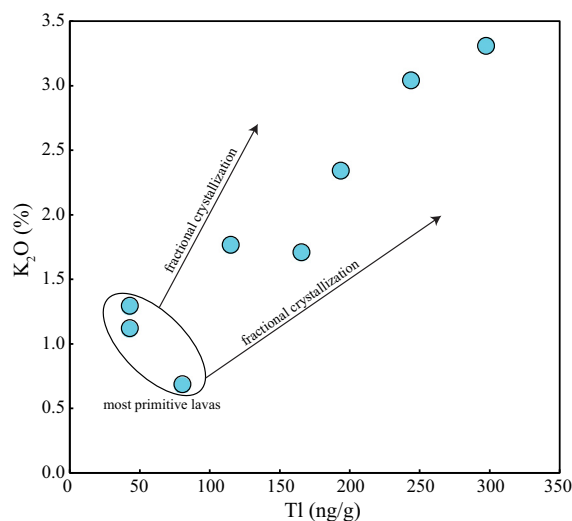
Fig. 5. Potassium plotted against Tl concentrations in lavas from Korovin volcano. Samples broadly follow a fractional crystallization trend. The two arrows indicate the evolution of primitive magmas from fractional crystallization assuming partition coefficients for K and Tl of 0.

Even though fractional crystallization and assimilation appears to have a limited effect on Tl isotopes, we still choose to exclude samples from the Eastern and Central Aleutian Islands that bear evidence of magmatic evolution (>55 wt% SiO_2, $<3\%$ MgO and Mg# <45) in order to remove any doubt that some Tl isotope variation could be caused by these processes. This step removes the three most evolved Korovin samples from consideration as well as one from Westdahl (SAR-4). It should be noted that all of the excluded samples display $\varepsilon^{205}Tl \sim -2$ (Table 2),

which could indicate that assimilation of the arc crust tends to add Tl with an isotope composition that is similar to continental crust. Hence, assimilation may possibly attenuate the Tl isotope variation of arc lavas.

One sample from the Western Aleutians (TN182_08_003) is unusually enriched in Tl compared with all other Aleutian samples (subaerial or submarine) investigated here. The sample displays Ce/Tl $\sim$ 35, a factor of about 4 lower than any other sample in this study. It also has the lightest Tl isotope composition measured for the Aleutians (ε^{205}Tl = −9.3) and the leaching experiments confirmed that this value was unlikely to be caused by seawater alteration (Table 3). Inspection of the sample in thin section did not reveal any alteration minerals. However, the sample contains abundant amphibole phenocrysts many of which have resorbed textures indicating that amphibole was first crystallized and then started re-dissolving back into the melt (Yogodzinski et al., 2015). TN182_08_003 is the only basalt sample recovered from the Western Aleutians, which exhibits this texture, which may indicate that the liquid line of decent was interrupted potentially by assimilation of wall rock. If the magma chamber that hosted the lava prior to eruption was relatively shallow in the upper few km of the crust then the wall rock could be composed of low-temperature altered volcanic rocks, which are known to carry high Tl concentrations and very light Tl isotope compositions (Nielsen et al., 2006c; Coggon et al., 2014). Such assimilation processes would likely not affect radiogenic isotope systems like Pb, Nd and Sr because low-temperature AOC is not significantly enriched in these elements compared with fresh basalt and does not possess radiogenic isotope compositions that deviate substantially from fresh MORB and thereby also the compositions of the primary magma. Strontium isotope ratios of basaltic oceanic crust do become more radiogenic when interacting with seawater, but the vast majority of Sr isotope data for AOC in the literature display ^{87}Sr/^{86}Sr $\sim$ 0.703–0.705 (Staudigel et al., 1995; Teagle et al., 2003), which is only slightly different to TN182_08_003 that exhibits ^{87}Sr/^{86}Sr = 0.7033. We, therefore, conclude that this sample has been contaminated by assimilation of low-temperature AOC at relatively shallow crustal depths prior to eruption and do not consider it further in our discussion of Aleutian sub-arc mantle processes.

6.2. Sediment controls Tl isotope variation in the Central and Eastern Aleutian Islands

Excluding the sample that shows evidence of degassing (SAR-17) as well as the more evolved lavas (SAR-4, and three Korovin lavas) does not change the range of Tl isotope compositions recorded in the Eastern and Central Aleutian samples (ε^{205}Tl = −3.8 to +2.6). We interpret these data as representative of the Tl isotope variation in the mantle sources of the Aleutian lavas investigated here. Only one sample (Kanaga S489, ε^{205}Tl = −3.8) is lighter than the normal mantle value of ε^{205}Tl = −2 ± 0.5 (Nielsen et al., 2006b,c, 2007) with 13 of the remaining 18 samples exhibiting Tl isotope compositions significantly heavier than normal mantle. The generally heavy Tl isotope

compositions of the lavas are similar to the Tl isotope variation in the sediments outboard of the Aleutian arc (Fig. 2), which clearly implicates sediments as a significant source of Tl in the Aleutians. In detail, however, there are some important systematic along-arc changes in Tl isotopes that provide clues to processes taking place in the sub-arc mantle.

As has been noted previously (Sun, 1980; Kay and Kay, 1994; Yogodzinski et al., 2011), the composition of sediment subducted underneath the Aleutian arc is expected to change from continental detrital in the east as represented by DSDP Site 178 toward compositions with a higher proportion of abyssal clay in the Central Aleutians. Here we have obtained the first data from a drill hole outboard of the Central Aleutians (ODP Hole 886C), which confirms that pelagic clays enriched in trace elements like Nd, Pb and Tl are common at this location. Thallium isotope compositions of sediments in DSDP Sites 178 and 183 and ODP Hole 886C conform to the expected relationship whereby sediments more proximal to the continent display ε^{205}Tl $\sim$ −2, with increasingly heavy Tl isotope compositions as sediment deposition rates decline and therefore contain higher concentrations of authigenic Fe and Mn oxides (Figs. 2 and 6).

The clear shift in Tl isotope composition of sediments from ε^{205}Tl $\sim$ −2 outboard of the Eastern Aleutians to ε^{205}Tl > 0 outboard of the Central Aleutians is mirrored by the average Tl isotope compositions of lavas in these locations (Figs. 7 and 8). Although each island appears to preserve some Tl isotope variation outside of analytical uncertainty (Figs. 7 and 8), on average, islands in the Central Aleutians exhibit heavier Tl isotope compositions than do the islands in the Eastern Aleutians. The relationship between Tl isotope compositions in subducted sediments and the extruded lavas indicates that sediment inputs are the main control on Tl isotope compositions of lavas in the Aleutians east of Kanaga Island. This interpretation is corroborated by the inverse correlation observed between Pb and Tl isotopes for the Central and Eastern Aleutian lavas (Fig. 7). It is important to note that this inverse correlation does not reflect two-component mixing, but that each point lies on an individual mixing line between the mantle wedge and a unique pelagic-detrital mix.

However, the observed trend is generally consistent with the Pb isotopes observed for pelagic clays at ODP 886C that are, on average, less radiogenic than the detrital-dominated sediments at DSDP Sites 178 and 183. Mixing lines between the sub-arc mantle and bulk detrital and pelagic sediments show that the quantity of sediment added from the slab to the sub-arc mantle decreases systematically from the Eastern to the Central Aleutians, which is consistent with the previously inferred subducted sediment flux along the Aleutian arc (Kay and Kay, 1994; Kelemen et al., 2003).

This trend is also reproduced in plots of Sr–Tl and Nd–Tl isotopes (Fig. 8), which shows that all four elements are likely dominated by sediment fluxes from the slab. The amount of bulk sediment required to account for the observed Nd, Pb, Sr and Tl isotope variations are consistently $\sim$0.6–1% by weight in the east, while mixing
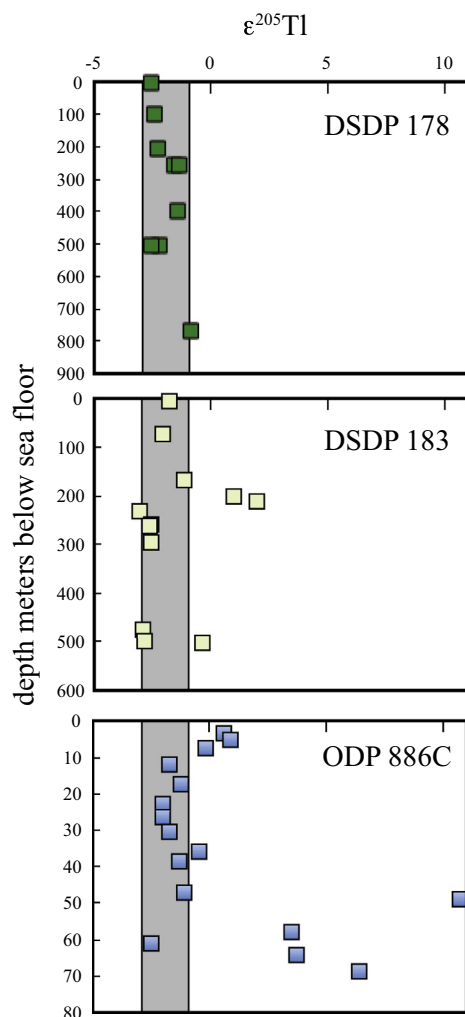
Fig. 6. Charts showing the Tl isotopic composition of sediments from the three drill holes investigated as a function of depth. It is evident that sediment cores located further west, and thereby more distally to the continent, contain more sections with Tl isotope compositions that are heavier than the continental crust. Grey bars denote the Tl isotope composition of the continental crust and upper mantle (Nielsen et al., 2005, 2006b).

relationships in the Central Aleutians using Nd, $^{206}Pb/^{204}Pb$, Sr and Tl isotopes are consistent with $\sim$0.2–0.6% by weight sediment addition, which is in reasonable agreement with previous work that inferred up to $\sim$2 wt% sediment in the mantle sources of the Aleutian Islands (Kay et al., 1978; Kay, 1980; Kay and Kay, 1988; Kelemen et al., 2003; Yogodzinski et al., 2011). Interestingly, bulk sediment mixing using $^{207}Pb/^{204}Pb$ and $^{208}Pb/^{204}Pb$ (Fig. 7b and c) predict significantly smaller (<0.2% by weight) pelagic sediment fractions in the Central Aleutians than do all other isotope ratios.

This consistent offset might be explained by addition of a third component with unradiogenic $^{207}Pb/^{204}Pb$ and $^{208}Pb/^{204}Pb$ such as a fluid from AOC (Miller et al., 1994). To maintain the consistent mixing relationships illustrated in Fig. 8, such a fluid would have to be highly enriched in Pb compared with Nd, Sr and Tl. In addition, the $^{206}Pb/^{204}Pb$ of the fluid could not be significantly less radiogenic than 18.6–18.7 in order to preserve the $\sim$0.4% pelagic sediment produced by the mixing relationship in Fig. 7a. Alternatively, it is also possible that the average subducted sediment outboard of the Central Aleutians is more affected by the type of highly enriched pelagic sediment represented by 886C-8H-4 58–60 cm (Table 4), which is characterized by highly unradiogenic $^{207}Pb/^{204}Pb$ and $^{208}Pb/^{204}Pb$, whereas $^{206}Pb/^{204}Pb$ is only slightly less radiogenic than most of the other pelagic sediment samples from ODP Hole 886C. Hence, if material similar to sample 8H-4 58–60 cm represents close to 60% of the subducted sediment Pb budget the bulk subducted sediment would be characterized by $^{207}Pb/^{204}Pb \sim 15.57$ and $^{208}Pb/^{204}Pb \sim 38.3$, which would yield mixing relationships requiring $\sim$0.4% bulk sediment like those observed for Nd, $^{206}Pb/^{204}Pb$, Sr and Tl isotopes. The present fraction of Pb in ODP Hole 886C contributed from the basal pelagic sediment is $\sim$35%, which is based on visual inspection of core barrel photographs (Rea et al., 1993). Although this method of estimating average sediment core compositions is the best available (short of conducting hundreds of individual sediment analyses throughout a core), it carries significant uncertainties for elements such as Pb, Tl, La and Nd that display almost two orders of magnitude concentration variations in individual sediment horizons. Hence, if the sediment thickness and/or average concentration of certain sediment horizons have been under- or overestimated this could lead to large changes in the whole-core average composition.

The similarity in the required sediment component based on Sr, Nd, Pb and Tl isotopes suggests that initial mixing between sediment and mantle does not strongly fractionate these four trace elements. However, it is well documented that Aleutian lavas (and arc lavas in general) display highly fractionated Sr/Nd and Pb/Nd compared with all the bulk input components that enter the subduction zone (Miller et al., 1994; Class et al., 2000). Therefore, there must be one or more processes occurring within the subduction zone that are capable of fractionating trace elements. Combining the evidence from isotope–isotope diagrams and the ubiquitous trace element fractionation in arcs would, therefore, suggest that mixing and trace element fractionation occur in two separate steps. The elemental fractionations of Sr/Nd, Ce/Pb, Th/Nd and others are often inferred to originate from melting or dehydration of slab sediment and/or altered oceanic crust with phases such as allanite, monazite, apatite, phengite, biotite, lawsonite or sulfide in the residue (Johnson and Plank, 1999; Hermann and Rubatto, 2009; Prytulak et al., 2013). These accessory phases could produce large variations in the transport efficiency of Sr, Nd, Pb and Tl, because of the strong compatibility of Nd in allanite and monazite, Pb in sulfide and apatite, and Tl in sulfide, biotite and phengite. Thus, sediment melts released from the slab into the mantle wedge are likely characterized by fractionated Sr/Nd, Pb/Tl, Sr/Tl and Nd/Tl ratios that would cause strong curvature in the isotope mixing diagrams (Figs. 7 and 8) that is not compatible with the consistent bulk mixing relationships observed.
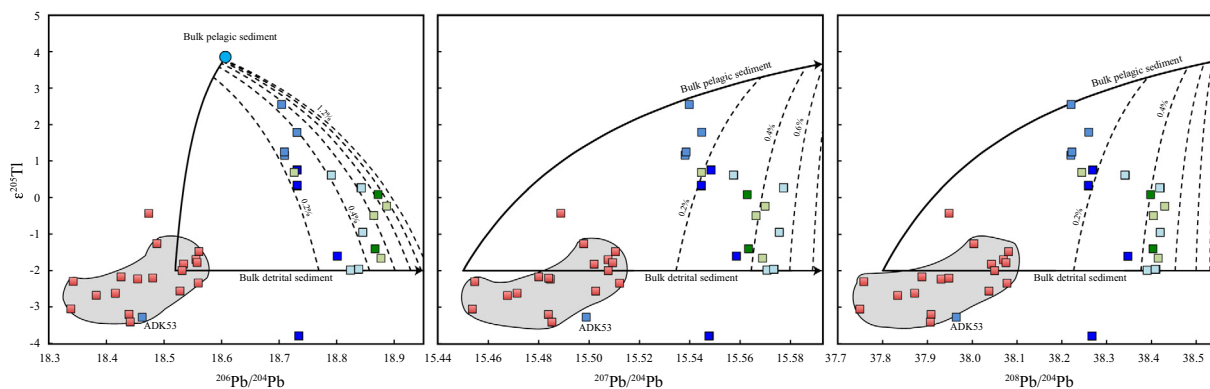
Fig. 7. Thallium isotopes plotted against Pb isotope ratios. Only samples that are not affected by subaerial weathering, assimilation, contamination or degassing are shown (see text for details). Symbol colors as in Fig. 3. Also shown are mixing lines between depleted mantle and bulk detrital (DSDP 178 and 183) and pelagic (ODP 886C) sediments. Dashed lines of constant sediment addition are indicated at 0.2% by weight intervals. The Pb isotope composition of the depleted mantle was taken from the most proximal MORB sample, which is from the northern Juan de Fuca ridge (Hegner and Tatsumoto, 1987). A Pb concentration of 28 ng/g for the DMM is used, which is based on $Ce/Tl_{DMM} = 1110$ and $Pb/Tl_{DMM} = 56$ (Nielsen et al., 2014) and a Ce concentration of 0.55 µg/g (Workman and Hart, 2005). The Tl isotope composition of the upper mantle is $\varepsilon^{205}Tl = -2$ (Nielsen et al., 2006b). The Pb isotope compositions and concentrations for detrital (DSDP 178 and 183) sediments were taken from (Plank and Langmuir, 1998), whereas Pb data for pelagic (ODP 886C) sediment as well as all sedimentary Tl data was taken from Table 5 in this study. (For interpretation of the references to color in this figure legend, the reader is referred to the web version of this article.)

Of the four isotope systems considered here, reliable experimental data for element partitioning during sediment melting only exists for Sr and Nd (Johnson and Plank, 1999; Hermann and Rubatto, 2009; Skora and Blundy, 2010). These data show that over a range of temperatures (600–1050 °C) and sediment compositions, Nd is preferentially retained in the sediment residue (notably by monazite), while Sr is uniformly released into the melt phase. On average, experiments in the temperature range from 700 to 900 °C show that Sr is about 20 times less compatible than Nd during sediment melting, which results in high Sr/Nd ratios in the sediment melts. A potential problem with these experiments is that they were all doped with relatively large amounts of Nd and other REE, which may have stabilized excess abundances of monazite because REE are a main constituent of the mineral. The Nd partition coefficients presented in these studies may, therefore, be higher than for undoped compositions. Irrespective of the absolute partition coefficients, sediment melts are expected to be characterized by higher Sr/Nd ratios than the bulk sediment, which generates significantly different mixing relationships between mantle and sediment melts compared to bulk sediment. Fig. 9 shows the effect of the different Nd/Sr ratios in bulk sediment and sediment melts generated by 20% melting of the subducted sediment components in the Eastern and Central Aleutians when using the experimental data currently available in the literature. It is evident that none of the lavas studied here nor those of other published lavas from the Central and Eastern Aleutians fall within the sediment melt field. Larger degrees of sediment melting (Skora and Blundy, 2010) will move the sediment melt field closer to the bulk sediment field, but even 40% sediment melting will only move a few of the samples into the sediment melt field and then only close to the mixing line with ODP 886C sediment melts.

On the other hand, if monazite abundances for un-doped sediment compositions are lower than doped experiments suggest, then it is likely that degrees of sediment melting around 20–40% will significantly attenuate the Sr/Nd fractionation of the sediment melt because the accessory phases responsible for the elemental fractionation are almost or entirely melted out (Hermann and Rubatto, 2009). In this case, sediment melts will fail to produce the high Sr/Nd ratios (and likely also other trace element ratios that might be governed by residual accessory phases) observed in Aleutian lavas and therefore processes subsequent to mantle-sediment melt mixing would be needed to fractionate trace element ratios like Sr/Nd, Ce/Pb, Cs/Tl and Th/Nd.

Bulk sediment transfer from slab to mantle wedge could be consistent with recent models of sediment transport from the slab to the mantle wedge whereby either pure sediment (Behn et al., 2011) or mélange diapirs (Marschall and Schumacher, 2012) are the primary mode of adding sediments and/or AOC to the source regions of arc lavas. Mélange formation at the slab–mantle interface, which based on field studies is common in subduction zones (Bebout, 1991; King et al., 2003), represents a mixture between slab material (both sediments and AOC) and the mantle wedge. Therefore, average mélange material is expected to plot along bulk mixing lines between mantle and sediment/AOC slab components, similar to what we observe in Figs. 7–9.

It is important to note that the isotope-isotope plots (Figs. 7–9) only provide information about the elemental ratios (e.g. Sr/Nd, Tl/Sr, Tl/Nd, Tl/Pb) at the time when the components mixed. Subsequent trace element fractionation would not be detected in these plots. In other words, models that invoke bulk mixing between mantle and sediment/AOC require that the strong fractionation of trace
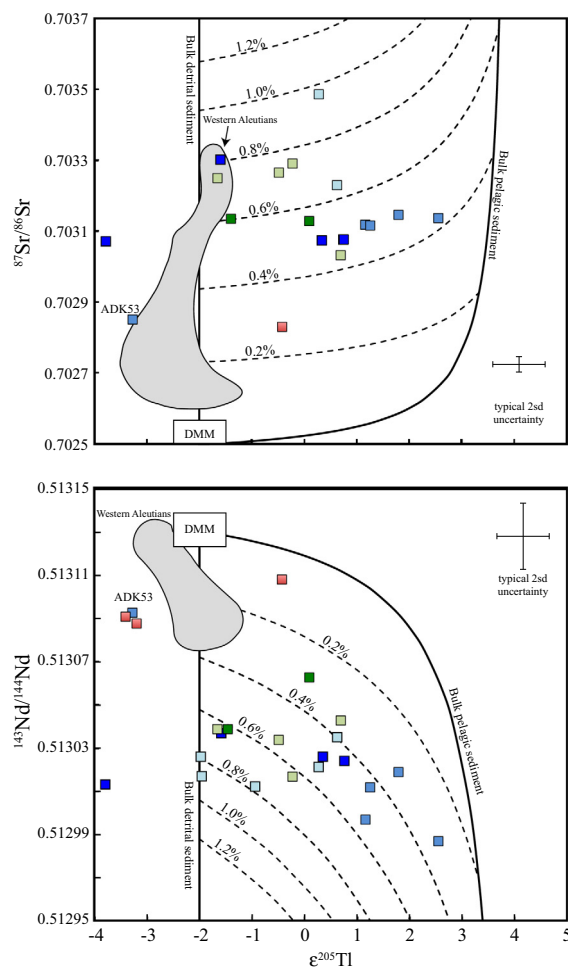
Fig. 8. Thallium isotopes plotted against (a) Sr and (b) Nd isotope ratios. Only samples that are not affected by subaerial weathering, assimilation, contamination or degassing are shown (see text for details). Symbol colors as in Fig. 3. Grey areas denote the Western Aleutian samples except one (for Sr isotopes) or three (for Nd isotopes) outliers. Also shown are mixing lines between depleted mantle and bulk detrital (DSDP 178 and 183) and pelagic (ODP 886C) sediments. Dashed lines of constant sediment addition are indicated at 0.2% by weight intervals. The Nd and Sr isotope composition of the depleted mantle was taken from the most proximal MORB sample, which is from the northern Juan de Fuca ridge (Hegner and Tatsumoto, 1987). Concentrations in the DMM of Sr = 7.66 µg/g and Nd = 0.58 µg/g were used, which were taken from Workman and Hart (2005). The Tl isotope composition of the upper mantle is $\varepsilon^{205}Tl = -2$ and the Tl content of the DMM was inferred from Pb/Tl ~ 56 (Nielsen et al., 2014). The Nd and Sr isotope compositions and concentrations for detrital (DSDP 178 and 183) sediments were taken from (Plank and Langmuir, 1998; Vervoort et al., 2011), whereas Nd and Sr data for pelagic (ODP 886C) sediment as well as all sedimentary Tl data was taken from Table 5 in this study. (For interpretation of the references to color in this figure legend, the reader is referred to the web version of this article.)

elements observed in arc lavas, including Sr/Nd, Ce/Pb and Nd/Th, must then occur upstream of the mixing process rather than prior to. Melting of mélange diapirs in the mantle wedge (Marschall and Schumacher, 2012) is a potential
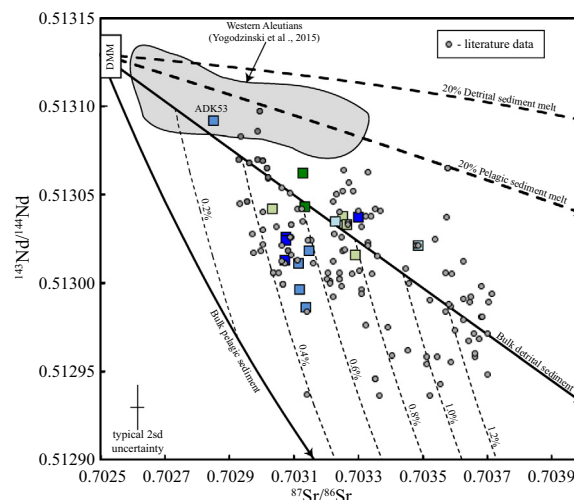
Fig. 9. Nd and Sr isotope compositions plotted against each other. Symbol colors as in Fig. 3, except the Western Aleutian samples that are denoted by grey area. Additional data from previous studies of the Aleutian Islands east of Kanaga are plotted for comparison (Class et al., 2000; George et al., 2003; Jicha et al., 2004; Singer et al., 2007; Yogodzinski et al., 2011). Also shown are mixing lines (bold lines) between depleted mantle and bulk detrital (DSDP 178 and 183) and pelagic (ODP 886C) sediments. Thin dashed lines of constant sediment addition are indicated at 0.2% by weight intervals. The Nd and Sr isotope composition of the depleted mantle was taken from the most proximal MORB sample, which is from the northern Juan de Fuca ridge (Hegner and Tatsumoto, 1987). Concentrations in the DMM of Sr = 7.66 µg/g and Nd = 0.58 µg/g were used, which were taken from Workman and Hart (2005). A second set of bold dashed mixing lines between DMM and sediment melts are also shown. These mixing lines were constructed by generating 20% melts from the detrital and pelagic sediment endmembers and using melt-residue partition coefficients of $D_{Sr} = 7.3$ and $D_{Nd} = 0.35$, which represents the average values recorded in sediment melting experiments by Hermann and Rubatto (2009) with temperatures from 750 to 900 °C. (For interpretation of the references to color in this figure legend, the reader is referred to the web version of this article.)

means of fractionating trace elements if melting residuals at high temperatures (likely >1100 °C) contains the residual phases that may produce the required trace element fractionations. Future experiments and studies of mélange material at subduction zone conditions will need to investigate the viability of these processes in more detail.

6.3. Thallium isotope signature of slab melts from altered oceanic crust

The Tl isotope ratios determined for samples from the Western Aleutians are systematically different from those observed in the Central and Eastern Aleutian Islands. When the two samples affected by assimilation and degassing (TN182_07_005 and TN182_08_003) are excluded, all samples except two fall within a limited range of $\varepsilon^{205}Tl = -1.5$ to -3.4 (Table 3). Even though this range only represents about four times our long-term reproducibility there is a suggestion that Tl isotopes correlate with both Sr and Pb isotopes, whereby the least radiogenic

Sr and Pb isotope compositions are characterized by ε^{205}Tl ~ -3.5 (Figs. 7 and 8). We also find that the Miocene sample from Adak Island, ADK53, falls close to these trends, suggesting that the Western Aleutian lavas were influenced by the same component as ADK53. There is strong evidence that the Western Aleutian lavas as well as ADK53 sample a distinct component of eclogite slab melt (Kay, 1978; Yogodzinski et al., 1995; Yogodzinski et al., 2015) that is characterized by high Sr/Y and Dy/Yb coupled with unradiogenic Pb and Sr isotope compositions. This eclogite melt likely originates from subducted basaltic oceanic crust that was transformed at depth to eclogite. Conversely, the lack of heavy Tl isotope compositions in the Western Aleutians indicate that sediments do not play a major role for the Tl mass balance of these lavas. This observation is consistent with the strongly attenuated sediment flux underneath the Western Aleutians (Yogodzinski et al., 1994; Kelemen et al., 2003) as well as radiogenic isotope compositions of Western Aleutian samples, which have among the least radiogenic Pb and most radiogenic Nd in the Aleutians. Nonetheless, plots of Pb–Pb and Nd–Pb isotopes as well as Ce/Pb significantly lower than normal mantle imply that minor sediment or fluid components are present in Western Aleutian samples (Yogodzinski et al., 2015). Therefore, simple mixing of melts from eclogitized oceanic crust and the mantle wedge cannot account for the petrogenesis of most Western Aleutian volcanics.

Thallium concentrations and isotope compositions of oceanic crust display distinct and systematic variations with crustal depth (Nielsen et al., 2006c). In particular, the upper volcanic zone is enriched in Tl with distinct ε^{205}Tl < -2. The sheeted dike complex, lower crustal gabbros and ultramafic cumulates, however, are likely very depleted in Tl and exhibit ε^{205}Tl ~ -2, which is indistinguishable from the MORB mantle (Nielsen et al., 2006c). In the Western Aleutian lavas, the proposed eclogite melt endmember is characterized by the lightest Tl isotope compositions suggesting that at least part of the eclogite source region formed from the volcanic zone of the subducted basaltic crust. This inference is also supported by the relatively high Tl concentrations for the putative eclogite component of up to 150 ng/g (Table 3), which would imply a source region containing Tl concentrations significantly in excess of the $\sim$1 ng/g Tl observed for the sheeted dike complex (Nielsen et al., 2006c).

One lava from Kanaga Island (S489) is the only sample from the main Aleutian Islands in this study that exhibits ε^{205}Tl < -2, which could be indicative of influence from low-temperature altered oceanic crust. There is no indication based on Sr/Y, Dy/Yb or radiogenic isotope ratios that a significant component derived from slab melting has influenced this sample. However, given the generally attenuated sediment flux needed to account for radiogenic isotope data from the Central Aleutians compared to the Eastern Aleutians (Figs. 7 and 8), it is possible that some volcanoes in the Central Aleutians become more dominated by inputs from dehydrated altered oceanic crust. Such an interpretation would be consistent with the greater range in Tl isotopes observed for Kanaga Island, which could reflect

that the relative contributions of Tl from sediments and altered oceanic crust are highly variable when the subducted sediment flux becomes sufficiently small.

6.4. Possible contributions from oceanic crust dehydration

Sediments have been widely implicated as the primary component that causes radiogenic Pb, Sr and Nd isotope variation in the Eastern and Central Aleutians (Kay et al., 1978; Kay and Kay, 1988; Kelemen et al., 2003), which is clearly supported by our new Tl isotope data (Figs. 7 and 8). However, fluids sourced from dehydrating oceanic crust as well as melts from eclogitized oceanic crust may also contribute to lavas in the Central and Eastern Aleutian Islands (Miller et al., 1994; Yogodzinski et al., 1995, 2015; Jicha et al., 2004; Singer et al., 2007). For example, several studies have suggested that a fluid extracted from AOC can account for the excess Sr in Aleutian lavas (Class et al., 2000; Jicha et al., 2004; Singer et al., 2007). This process is clearly a reasonable way to explain the trace element fractionation of several key trace elements (notably the high Sr/Nd, Pb/Ce and B/La). However, addition of an AOC component would cause Sr isotopes to become slightly more radiogenic (assuming ^{87}Sr/^{86}Sr ~ 0.704 in the upper ~ 600 m of the oceanic crust (Staudigel et al., 1995; Teagle et al., 2003)) whereas Nd would be largely unaffected due to the low solubility of Nd in the fluid phase (Kessel et al., 2005). Adding this 'fluid AOC' component to the sediment melt would move the sediment melt-mantle mixing lines in Fig. 9 upwards and therefore even further away from the sediment melt field. On the other hand, if 'fluid AOC' Sr were derived from throughout the oceanic crust (with MORB ^{87}Sr/^{86}Sr ~ 0.7025) and this fluid exhibited elevated Sr/Nd similar to low degree ($<20\%$) sediment melts, then a mixing line could be produced that is indistinguishable from mantle-bulk sediment mixing, and would intersect the Aleutian arc data. Hence, low degree ($<20\%$) sediment melts are able to explain the Sr-Nd isotope data from the Aleutian arc if they were mixed with AOC fluids characterized by MORB isotope compositions and Sr/Nd ratios similar to the sediment melt. However, this scenario would require that less than 15% of Sr in the Aleutian lavas are derived from the mantle, as otherwise the mixing lines would become too curved to encompass all the isotopic data.

It is currently unknown how mobile Tl is in fluids released from the subducting slab and, therefore, it is difficult to quantify what the effect on Tl isotopes and abundances would be if Aleutian lavas contained a significant fluid component from altered oceanic crust. We can obtain qualitative information by examining the relation between the highly fluid mobile element Cs (Melzer and Wunder, 2000; Kessel et al., 2005) and Tl across the Aleutian arc (Fig. 10). All bulk endmembers in the Aleutian arc (e.g. mantle wedge, detrital and pelagic sediments, altered oceanic crust and slab melts) display Cs/Tl < 10, while lavas from the Central and Eastern Aleutian Islands display Cs/Tl = 8–35. Although Cs and Tl do not partition identically during mantle melting (Nielsen et al., 2014), they are both so incompatible that mantle melts representing $>5\%$
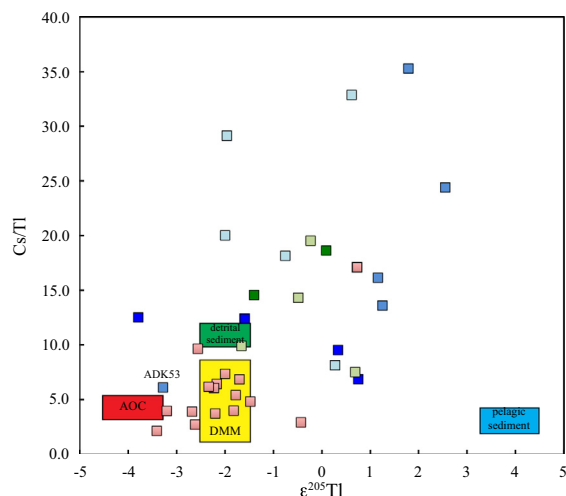
Fig. 10. Thallium isotope compositions plotted against Cs/Tl ratio for Aleutian lavas from this study. Only samples that are not affected by subaerial weathering, assimilation, contamination or degassing are shown (see text for details). Symbol colors as in Fig. 3. Also shown are the values for detrital (DSDP 178 and 183) and pelagic (ODP 886C) sediments as well as an estimated value for altered oceanic crust (AOC) (Nielsen et al., 2006c) and the DMM (Nielsen et al., 2006b, 2014). It is notable that many of the Central and Eastern Aleutian lavas display Cs/Tl higher than any of the bulk components contributing to the lavas. This effect could either be explained by the involvement of Cs-rich fluids or preferential retention of Tl in phengite (see text for details). (For interpretation of the references to color in this figure legend, the reader is referred to the web version of this article.)

melting are not significantly fractionated from their mantle source. Thallium concentration data from a range of arcs indicates that Tl is only mildly fluid mobile (Noll et al., 1996) and, therefore, fluid dominated arc lavas should display high Cs/Tl. Thus, the high Cs/Tl in Aleutian lavas are potentially caused by addition of a fluid with high Cs/Tl to the magma source region. Alternatively, the high Cs/Tl could be explained by a residual phase in the mantle wedge or the slab that retains Tl over Cs. This residual phase could for example be sulfide or phengite, both of which are expected to accommodate Tl (Kiseeva and Wood, 2013; Prytulak et al., 2013; Nielsen et al., 2014). Phengite also incorporates Cs, but it has been shown that Cs is the least compatible alkali metal in phengite (Melzer and Wunder, 2000; Hermann and Rubatto, 2009) due to its slightly larger ionic radius than the alkali metal cation site in phengite (Busigny et al., 2003). The ionic radius of Tl is very similar to that of Rb (Shannon, 1976), which should render Tl significantly more compatible in phengite than Cs. Thus, high Cs/Tl in arc lavas could be due to phengite retention in the slab as well as residual sulfide in the mantle wedge. However, future experimental work must be conducted in order to verify this inference.

Conversely, lavas from the Western Aleutians exhibit Cs/Tl that overlaps with MORB (Fig. 10) suggesting that the high Cs/Tl component in the main Aleutian Islands is largely absent in the Western Aleutians. Considering that sediment contributions are likely small in the Western

Aleutians (Yogodzinski et al., 1994, 2015; Kelemen et al., 2003), it follows that the high Cs/Tl ratios in the main Aleutian Islands probably originate from the sediment component rather than fluids released from altered oceanic crust. This conclusion is supported by the weak tendency for Eastern and Central Aleutian lavas with heavy Tl isotope compositions to display the highest Cs/Tl (Fig. 10). It should be noted that the process that generated high Cs/Tl in the Aleutian lavas, be it fluid driven or mineralogical, would still need to occur after bulk mixing between the sediment and mantle components due to the mixing relations observed between Tl–Sr–Nd–Pb isotopes (Figs. 7–9). However, given the lack of Tl partitioning data for phengite and subduction fluids it is presently not possible to conclude if fluids are necessary to account for the Cs/Tl ratios observed in the Aleutian lavas.

7. CONCLUSIONS

We have conducted the first Tl isotope study of lavas covering the entire Aleutian arc and subducting sediments located outboard of the main Aleutian Islands. Systematic changes are observed in the average sediment Tl isotope composition from $\varepsilon^{205}Tl \sim -2$, similar to the continental crust and upper mantle, in the Eastern Aleutians to $\varepsilon^{205}Tl \sim +4$ in the Central Aleutians, which reflects a significant component of authigenic Mn oxides in these slowly accumulating sediments. Lavas in the Aleutian Islands east of Kanaga generally mirror the trend from $\varepsilon^{205}Tl \sim -2$ in the Eastern Aleutians to $\varepsilon^{205}Tl \sim +2$ in the Central Aleutians caused by the changing subducted sediment composition across the arc. Simple models of sediment-mantle mixing in Nd, Pb, Sr and Tl isotope space reveal that bulk sediment mixed with a depleted mantle source can account for the isotopic variation observed in the Central and Eastern Aleutian Islands. Our results are, therefore, consistent with recent models of sediment transport from the slab to the mantle wedge whereby either pure sediment (Behn et al., 2011) or mélange diapirs (Marschall and Schumacher, 2012) are the primary mode of adding sediments to the source regions of arc lavas. However, bulk sediment mixing models require that processes occurring after sediment-mantle mixing fractionate trace element ratios such as Ce/Pb, Cs/Tl, Sr/Nd, and Th/Nd. Both the sediment and mélange diapir models have not been explored in terms of the resulting chemical signatures that can be generated in these scenarios. For example, it is not clear if sediment diapirs need to melt first in order to effectively mix with the mantle wedge in which case trace element fractionation would likely occur prior to mixing and, therefore, not adequately explain the isotope–isotope relationships (Fig. 9). The strong heterogeneity of mélange zones sometimes observed in the field (Bebout, 2007) is perhaps not compatible with the relatively homogenous isotopic signatures often observed for individual aleutian volcanoes (Kelemen et al., 2003). Lastly, the high temperatures (>1100 °C) potentially experienced by sediment and mélange diapirs in the mantle wedge could prevent significant trace element fractionation as accessory phases might melt out and therefore not generate the required trace element

fractionation. Future experiments that reproduce the conditions experienced in sediment and mélange diapirs will need to investigate the viability of these processes in generating the observed major and trace element characteristics of arc lavas.

Alternative models that involve sediment melting in excess of 50% may also be compatible with the presented Nd, Pb, Sr and Tl isotopes. Such large degrees of melting could be driven by an influx of AOC fluid with MORB-like isotope compositions (Skora and Blundy, 2010), which may also deliver fractionated trace elements. Provided the sediment melt and AOC fluid had similar trace element ratios, they have the potential to produce arrays that look like bulk mixing but also generate trace element fractionations (e.g., high Sr/Nd, Cs/Tl and Pb/Ce) observed in arc lavas.

Thallium isotope systematics in Western Aleutian lavas show compositions slightly lighter than the upper mantle, which implies a negligible sediment flux at this location and probably involvement of low-temperature altered oceanic crust in the generation of these lavas. In general, the lightest Tl isotope compositions are observed for the highest Sr/Y ratios and most unradiogenic Sr and Pb isotope compositions, which may be consistent with derivation of these lavas via melting of eclogitized altered oceanic crust.

ACKNOWLEDGEMENTS

APPENDIX A. SUPPLEMENTARY DATA

Supplementary data associated with this article can be found, in the online version, at http://dx.doi.org/10.1016/j.gca.2016.03.010.

REFERENCES

Abouchami W., Galer S. J. G. and Koschinsky A. (1999) Pb and Nd isotopes in NE Atlantic Fe–Mn crusts: proxies for trace metal paleosources and paleocean circulation. *Geochim. Cosmochim. Acta* **63**, 1489–1505.

Adam J. and Green T. (2006) Trace element partitioning between mica- and amphibole-bearing garnet lherzolite and hydrous basanitic melt: 1. Experimental results and the investigation of controls on partitioning behaviour. *Contrib. Mineral. Petrol.* **152**, 1–17.

Baker R. G. A., Rehkämper M., Hinkley T. K., Nielsen S. G. and Toutain J. P. (2009) Investigation of thallium fluxes from subaerial volcanism – implications for the present and past mass balance of thallium in the oceans. *Geochim. Cosmochim. Acta* **73**, 6340–6359.

Bebout G. E. (1991) Field-based evidence for devolatilization in subduction zones – implications for arc magmatism. *Science* **251**, 413–416.

Bebout G. E. (2007) Metamorphic chemical geodynamics of subduction zones. *Earth Planet. Sci. Lett.* **260**, 373–393.

Behn M. D., Kelemen P. B., Hirth G., Hacker B. R. and Massonne H. J. (2011) Diapirs as the source of the sediment signature in arc lavas. *Nat. Geosci.* **4**, 641–646.

Ben Othmann D., White W. M. and Patchett J. (1989) The geochemistry of marine sediments, island arc magma genesis, and crust-mantle recycling. *Earth Planet. Sci. Lett.* **94**, 1–21.

Busigny V., Cartigny P., Philippot P., Ader M. and Javoy M. (2003) Massive recycling of nitrogen and other fluid-mobile elements (K, Rb, Cs, H) in a cold slab environment: evidence from HP to UHP oceanic metasediments of the Schistes Lustres nappe (western Alps, Europe). *Earth Planet. Sci. Lett.* **215**, 27–42.

Byrne R. H. (2002) Inorganic speciation of dissolved elements in seawater: the influence of pH on concentration ratios. *Geochem. Trans.* **3**, 11–16.

Carpentier M., Chauvel C. and Mattielli N. (2008) Pb–Nd isotopic constraints on sedimentary input into the Lesser Antilles arc system. *Earth Planet. Sci. Lett.* **272**, 199–211.

Carter L. B., Skora S., Blundy J. D., De Hoog J. C. M. and Elliott T. (2015) An experimental study of trace element fluxes from subducted oceanic crust. *J. Petrol.* **56**, 1585–1605.

Class C., Miller D. M., Goldstein S. L. and Langmuir C. H. (2000) Distinguishing melt and fluid subduction components in Umnak Volcanics, Aleutian Arc. *Geochem. Geophys. Geosyst.* **1**. http://dx.doi.org/10.1029/1999GC000010.

Coggon R. M., Rehkämper M., Atteck C., Teagle D. A. H., Alt J. C. and Cooper M. J. (2014) Mineralogical and microbial controls on thallium uptake during hydrothermal alteration of the upper ocean crust. *Geochim. Cosmochim. Acta* **144**, 25–42.

Defant M. J. and Drummond M. S. (1990) Derivation of some modern arc magmas by melting of young subducted lithosphere. *Nature* **347**, 662–665.

George R., Turner S., Hawkesworth C., Morris J., Nye C., Ryan J. and Zheng S. H. (2003) Melting processes and fluid and sediment transport rates along the Alaska-Aleutian arc from an integrated U–Th–Ra–Be isotope study. *J. Geophys. Res.-Solid Earth*, 108.

Hegner E. and Tatsumoto M. (1987) Pb, Sr, and Nd isotopes in basalts and sulfides from the Juan-De-Fuca Ridge. *J. Geophys. Res.-Solid Earth Planets* **92**, 11380–11386.

Hein J. R., Koschinsky A., Bau M., Manheim F. T., Kang J.-K. and Roberts L. (2000) Cobalt-rich ferromanganese crusts in the Pacific. In *Handbook of Marine Mineral Deposits* (ed. D. S. Cronan). CRC Press, Boca Raton, pp. 239–280.

Heinrichs H., Schulz-Dobrick B. and Wedepohl K. H. (1980) Terrestrial geochemistry of Cd, Bi, Tl, Pb, Zn and Rb. *Geochim. Cosmochim. Acta* **44**, 1519–1533.

Hermann J. (2002) Allanite: thorium and light rare earth element carrier in subducted crust. *Chem. Geol.* **192**, 289–306.

Hermann J. and Rubatto D. (2009) Accessory phase control on the trace element signature of sediment melts in subduction zones. *Chem. Geol.* **265**, 512–526.

Jackson M. G. and Hart S. R. (2006) Strontium isotopes in melt inclusions from Samoan basalts: implications for heterogeneity in the Samoan plume. *Earth Planet. Sci. Lett.* **245**, 260–277.

Jenner F. E. and O'Neill H. S. C. (2012) Analysis of 60 elements in 616 ocean floor basaltic glasses. *Geochem. Geophys. Geosyst.* **13**.

Jicha B. R., Singer B. S., Brophy J. G., Fournelle J. H., Johnson C. M., Beard B. L., Lapen T. J. and Mahlen N. J. (2004) Variable impact of the subducted slab on Aleutian island arc magma sources: evidence from Sr, Nd, Pb, and Hf isotopes and trace element abundances. *J. Petrol.* **45**, 1845–1875.

Jochum K. P. and Verma S. P. (1996) Extreme enrichment of Sb, Tl and other trace elements in altered MORB. *Chem. Geol.* **130**, 289–299.

Johnson M. C. and Plank T. (1999) Dehydration and melting experiments constrain the fate of subducted sediments. *Geochem. Geophys. Geosyst.* **1**.

Kay R. W. (1978) Aleutian magnesian andesites – melts from subducted Pacific ocean crust. *J. Volcanol. Geotherm. Res.* **4**, 117–132.

Kay R. W. (1980) Volcanic arc magmas – implications of a melting-mixing model for element recycling in the crust-upper mantle system. *J. Geol.* **88**, 497–522.

Kay R. W. and Kay S. M. (1988) Crustal recycling and the Aleutian Arc. *Geochim. Cosmochim. Acta* **52**, 1351–1359.

Kay S. M. and Kay R. W. (1994) Aleutian magmas in space and time. In *The Geology of Alaska* (eds. G. Plafker and H. C. Berg). Geological Society of America, pp. 687–722.

Kay R. W., Sun S. S. and Lee-Hu C. N. (1978) Pb and Sr isotopes in volcanic rocks from the Aleutian Islands and Pribilof Islands, Alaska. *Geochim. Cosmochim. Acta.* **42**, 263–273.

Kelemen P. B., Yogodzinski G. M. and Scholl D. W. (2003) Along-strike variation in lavas of the Aleutian Island arc: implications for the genesis of high Mg# andesite and the continental crust. *Geophys. Monogr.* **138**, 223–276.

Kessel R., Schmidt M. W., Ulmer P. and Pettke T. (2005) Trace element signature of subduction-zone fluids, melts and super-critical liquids at 120–180 km depth. *Nature* **437**, 724–727.

King R. L., Kohn M. J. and Eiler J. M. (2003) Constraints on the petrologic structure of the subduction zone slab-mantle interface from Franciscan Complex exotic ultramafic blocks. *Geol. Soc. Am. Bull.* **115**, 1097–1109.

Kiseeva E. S. and Wood B. J. (2013) A simple model for chalcophile element partitioning between sulphide and silicate liquids with geochemical applications. *Earth Planet. Sci. Lett.* **383**, 68–81.

Ling H. F., Burton K. W., Onions R. K., Kamber B. S., vonBlanckenburg F., Gibb A. J. and Hein J. R. (1997) Evolution of Nd and Pb isotopes in Central Pacific seawater from ferromanganese crusts. *Earth Planet. Sci. Lett.* **146**, 1–12.

Ling H. F., Jiang S. Y., Frank M., Zhou H. Y., Zhou F., Lu Z. L., Chen X. M., Jiang Y. H. and Ge C. D. (2005) Differing controls over the Cenozoic Pb and Nd isotope evolution of deepwater in the central North Pacific Ocean. *Earth Planet. Sci. Lett.* **232**, 345–361.

Lugmair G. W. and Galer S. J. G. (1992) Age and isotopic relationships among the Angrites Lewis Cliff-86010 and Angra-Dos-Reis. *Geochim. Cosmochim. Acta* **56**, 1673–1694.

Marschall H. R. and Schumacher J. C. (2012) Arc magmas sourced from melange diapirs in subduction zones. *Nat. Geosci.* **5**, 862–867.

Melzer S. and Wunder B. (2000) Island-arc basalt alkali ratios: constraints from phengite-fluid partitioning experiments. *Geology* **28**, 583–586.

Miller D. M., Goldstein S. L. and Langmuir C. H. (1994) Cerium lead and lead-isotope ratios in arc magmas and the enrichment of lead in the continents. *Nature* **368**, 514–520.

Morris J. D., Leeman W. P. and Tera F. (1990) The subducted component in island-arc lavas – constraints from Be isotopes and B-Be systematics. *Nature* **344**, 31–36.

Nielsen S. G. and Rehkämper M. (2011) Thallium isotopes and their application to problems in earth and environmental science. In *Handbook of Environmental Isotope Geochemistry* (ed. M. Baskaran). Springer, pp. 247–270.

Nielsen S. G., Rehkämper M., Baker J. and Halliday A. N. (2004) The precise and accurate determination of thallium isotope compositions and concentrations for water samples by MC-ICPMS. *Chem. Geol.* **204**, 109–124.

Nielsen S. G., Rehkämper M., Porcelli D., Andersson P., Halliday A. N., Swarzenski P. W., Latkoczy C. and Gunther D. (2005)

Thallium isotope composition of the upper continental crust and rivers – an investigation of the continental sources of dissolved marine thallium. *Geochim. Cosmochim. Acta* **69**, 2007–2019.

Nielsen S. G., Rehkämper M. and Halliday A. N. (2006a) Large thallium isotopic variations in iron meteorites and evidence for lead-205 in the early solar system. *Geochim. Cosmochim. Acta* **70**, 2643–2657.

Nielsen S. G., Rehkämper M., Norman M. D., Halliday A. N. and Harrison D. (2006b) Thallium isotopic evidence for ferromanganese sediments in the mantle source of Hawaiian basalts. *Nature* **439**, 314–317.

Nielsen S. G., Rehkämper M., Teagle D. A. H., Alt J. C., Butterfield D. and Halliday A. N. (2006c) Hydrothermal fluid fluxes calculated from the isotopic mass balance of thallium in the ocean crust. *Earth Planet. Sci. Lett.* **251**, 120–133.

Nielsen S. G., Rehkämper M., Brandon A. D., Norman M. D., Turner S. and O'Reilly S. Y. (2007) Thallium isotopes in Iceland and Azores lavas – implications for the role of altered crust and mantle geochemistry. *Earth Planet. Sci. Lett.* **264**, 332–345.

Nielsen S. G., Mar-Gerrison S., Gannoun A., LaRowe D., Klemm V., Halliday A. N., Burton K. W. and Hein J. R. (2009) Thallium isotope evidence for a permanent increase in marine organic carbon export in the early Eocene. *Earth Planet. Sci. Lett.* **278**, 297–307.

Nielsen S. G., Gannoun A., Marnham C., Burton K. W., Halliday A. N. and Hein J. R. (2011) New age for ferromanganese crust 109D-C and implications for isotopic records of lead, neodymium, hafnium, and thallium in the Pliocene Indian Ocean. *Paleoceanography* **26**, PA2213, doi:2210.1029/2010PA002003.

Nielsen S. G., Wasylenki L. E., Rehkämper M., Peacock C. L., Xue Z. and Moon E. M. (2013) Towards an understanding of thallium isotope fractionation during adsorption to manganese oxides. *Geochim. Cosmochim. Acta* **117**, 252–265.

Nielsen S. G., Shimizu N., Lee C. T. A. and Behn M. (2014) Chalcophile behavior of thallium during MORB melting and implications for the sulfur content of the mantle. *Geochem. Geophys. Geosyst.* **15**, 4905–4919.

Nielsen S. G., Klein F., Kading T., Blusztajn J. and Wickham K. (2015) Thallium as a tracer of fluid-rock interaction in the shallow mariana forearc. *Earth Planet. Sci. Lett.* **430**, 416–426.

Noll P. D., Newsom H. E., Leeman W. P. and Ryan J. G. (1996) The role of hydrothermal fluids in the production of subduction zone magmas: evidence from siderophile and chalcophile trace elements and boron. *Geochim. Cosmochim. Acta* **60**, 587–611.

Peacock C. L. and Moon E. M. (2012) Oxidative scavenging of thallium by birnessite: controls on thallium sorption and stable isotope fractionation in marine ferromanganese precipitates. *Geochim. Cosmochim. Acta* **84**, 297–313.

Plank T. (2005) Constraints from thorium/lanthanum on sediment recycling at subduction zones and the evolution of the continents. *J. Petrol.* **46**, 921–944.

Plank T. and Langmuir C. H. (1998) The chemical composition of subducting sediment and its consequences for the crust and mantle. *Chem. Geol.* **145**, 325–394.

Prytulak J., Nielsen S. G., Plank T., Barker M. and Elliott T. (2013) Assessing the utility of thallium and thallium isotopes for tracing subduction zone inputs to the Mariana arc. *Chem. Geol.* **345**, 139–149.

Rabinowitz H. S., Savage H. M., Plank T., Polissar P. J., Kirkpatrick J. D. and Rowe C. D. (2015) Multiple major faults at the Japan Trench: chemostratigraphy of the plate boundary at iodp exp. 343: JFAST. *Earth Planet. Sci. Lett.* **423**, 57–66.

Rea D. K., Basov I. A., Janecek T. R. and Palmer-Julson A. (1993) Sites 885/886. *Proceedings of the Ocean Drilling Program, Initial Reports* **145**, 303–334.

Rehkämper M. and Halliday A. N. (1999) The precise measurement of Tl isotopic compositions by MC-ICPMS: application to the analysis of geological materials and meteorites. *Geochim. Cosmochim. Acta* **63**, 935–944.

Rehkämper M., Frank M., Hein J. R., Porcelli D., Halliday A., Ingri J. and Liebetrau V. (2002) Thallium isotope variations in seawater and hydrogenetic, diagenetic, and hydrothermal ferromanganese deposits. *Earth Planet. Sci. Lett.* **197**, 65–81.

Rehkämper M., Frank M., Hein J. R. and Halliday A. (2004) Cenozoic marine geochemistry of thallium deduced from isotopic studies of ferromanganese crusts and pelagic sediments. *Earth Planet. Sci. Lett.* **219**, 77–91.

Ryan J. G. and Chauvel C. (2014) 3.13 – the subduction-zone filter and the impact of recycled materials on the evolution of the mantle. In *Treatise on Geochemistry (Second Edition)* (ed. H. D. H. K. Turekian). Elsevier, Oxford, pp. 479–508.

Schauble E. A. (2007) Role of nuclear volume in driving equilibrium stable isotope fractionation of mercury, thallium, and other very heavy elements. *Geochim. Cosmochim. Acta* **71**, 2170–2189.

Scher H. D. and Delaney M. L. (2010) Breaking the glass ceiling for high resolution Nd isotope records in early Cenozoic paleoceanography. *Chem. Geol.* **269**, 329–338.

Schiano P., Dupré B. and Lewin E. (1993) Application of element concentration variability to the study of basalt alteration (Fangataufa atoll, French Polynesia). *Chem. Geol.* **104**, 99–124.

Shannon R. D. (1976) Revised effective ionic radii and systematic studies of interatomic distances in halides and chalcogenides. *Acta Crystallogr. A* **A32**, 751–767.

Shaw D. M. (1952) The geochemistry of thallium. *Geochim. Cosmochim. Acta* **2**, 118–154.

Singer B. S., Jicha B. R., Leeman W. P., Rogers N. W., Thirlwall M. F., Ryan J. and Nicolaysen K. E. (2007) Along-strike trace element and isotopic variation in Aleutian Island arc basalt: subduction melts sediments and dehydrates serpentine. *J. Geophys. Res.-Solid Earth*, 112.

Skora S. and Blundy J. (2010) High-pressure hydrous phase relations of radiolarian clay and implications for the involvement of subducted sediment in arc magmatism. *J. Petrol.* **51**, 2211–2243.

Snoeckx H., Rea D. K., Jones C. E. and Lynn Ingram B. (1995) Eolian and silica deposition in the central north pacific: results from sites 885/886. *Proc. ODP Sci. Results* **145**, 219–230.

Staudigel H., Davies G. R., Hart S. R., Marchant K. M. and Smith B. M. (1995) Large scale isotopic Sr, Nd and O isotopic anatomy of altered oceanic crust: DSDP/ODP sites 417/418. *Earth Planet. Sci. Lett.* **130**, 169–185.

Sun S. S. (1980) Lead isotopic study of young volcanic-rocks from mid-ocean ridges, ocean islands and island arcs. *Philos. Trans. R. Soc. London, Ser. A* **297**, 409–445.

Tanaka T., Togashi S., Kamioka H., Amakawa H., Kagami H., Hamamoto T., Yuhara M., Orihashi Y., Yoneda S., Shimizu H., Kunimaru T., Takahashi K., Yanagi T., Nakano T., Fujimaki H., Shinjo R., Asahara Y., Tanimizu M. and Dragusanu C. (2000) JNdi-1: a neodymium isotopic reference in consistency with LaJolla neodymium. *Chem. Geol.* **168**, 279–281.

Teagle D. A. H., Bickle M. J. and Alt J. C. (2003) Recharge flux to ocean-ridge black smoker systems: a geochemical estimate from ODP Hole 504B. *Earth Planet. Sci. Lett.* **210**, 81–89.

Tera F., Brown L., Morris J., Sacks I. S., Klein J. and Middleton R. (1986) Sediment incorporation in island-arc magmas - inferences from be-10. *Geochim. Cosmochim. Acta* **50**, 535–550.

Thirlwall M. F., Graham A. M., Arculus R. J., Harmon R. S. and Macpherson C. G. (1996) Resolution of the effects of crustal assimilation, sediment subduction, and fluid transport in island arc magmas: Pb–Sr–Nd–O isotope geochemistry of Grenada, Lesser Antilles. *Geochim. Cosmochim. Acta* **60**, 4785–4810.

Todt W., Cliff R. A., Hanser A. and Hofmann A. W. (1996) Evaluation of a 202Pb–205Pb double spike for high-precision lead isotope analysis. *Am. Geophys. Union Monogr.* **95**, 429–437.

Vervoort J. D., Plank T. and Prytulak J. (2011) The Hf–Nd isotopic composition of marine sediments. *Geochim. Cosmochim. Acta* **75**, 5903–5926.

Von Drach V., Marsh B. D. and Wasserburg G. J. (1986) Nd and Sr isotopes in the Aleutians – multicomponent parenthood of island-arc magmas. *Contrib. Mineral. Petrol.* **92**, 13–34.

Von Huene R. and Scholl D. W. (1991) Observations at convergent margins concerning sediment subduction, subduction erosion, and the growth of continental-crust. *Rev. Geophys.* **29**, 279–316.

Wedepohl K. H. (1995) The composition of the continental crust. *Geochim. Cosmochim. Acta* **59**, 1217–1232.

Weis D., Kieffer B., Maerschalk C., Pretorius W. and Barling J. (2005) High-precision Pb–Sr–Nd–Hf isotopic characterization of USGS BHVO-1 and BHVO-2 reference materials. *Geochem. Geophys. Geosyst.* **6**, 12–15.

Weis D., Kieffer B., Maerschalk C., Barling J., de Jong J., Williams G. A., Hanano D., Pretorius W., Mattielli N., Scoates J. S., Goolaerts A., Friedman R. M. and Mahoney J. B. (2006) High-precision isotopic characterization of USGS reference materials by TIMS and MC-ICP-MS. *Geochem. Geophys. Geosyst.* **7**.

White W. M. and Dupré B. (1986) Sediment subduction and magma genesis in the Lesser Antilles: isotopic and trace element constraints. *J. Geophys. Res.* **91**, 5927–5941.

Workman R. K. and Hart S. R. (2005) Major and trace element composition of the depleted MORB mantle (DMM). *Earth Planet. Sci. Lett.* **231**, 53–72.

Yogodzinski G. M., Volynets O. N., Koloskov A. V., Seliverstov N. I. and Matvenkov V. V. (1994) Magnesian andesites and the subduction component in a strongly calc-alkaline series at Piip Volcano, Far Western Aleutians. *J. Petrol.* **35**, 163–204.

Yogodzinski G. M., Kay R. W., Volynets O. N., Koloskov A. V. and Kay S. M. (1995) Magnesian andesite in the western aleutian Komandorsky region – implications for slab melting and processes in the mantle wedge. *Geol. Soc. Am. Bull.* **107**, 505–519.

Yogodzinski G. M., Lees J. M., Churikova T. G., Dorendorf F., Woerner G. and Volynets O. N. (2001) Geochemical evidence for the melting of subducting oceanic lithosphere at plate edges. *Nature* **409**, 500–504.

Yogodzinski G. M., Vervoort J. D., Brown S. T. and Gerseny M. (2011) Subduction controls of Hf and Nd isotopes in lavas of the Aleutian island arc. *Earth Planet. Sci. Lett.* **300**, 226–238.

Yogodzinski G. M., Brown S. T., Kelemen P. B., Vervoort J. D., Portnyagin M., Sims K. W. W., Hoernle K., Jicha B. R. and Werner R. (2015) The role of subducted basalt in the source of island arc magmas: evidence from seafloor lavas of the Western Aleutians. *J. Petrol.* **56**, 441–492.

Associate editor: Marc Norman